Combined Quantum Chemical/RRKM-ME Computational Study of the Phenyl + Ethylene, Vinyl + Benzene, and H + Styrene Reactions[†]

I. V. Tokmakov and M. C. Lin*

Department of Chemistry, Emory University, Atlanta, Georgia 30322, USA

Received: January 5, 2004; In Final Form: April 6, 2004

Reactions of phenyl radicals with ethylene (R1), vinyl radicals with benzene (R2), and H-atoms with styrene (R3) are important prototype processes pertinent to the formation and degradation of aromatic hydrocarbons in high-temperature environments. Detailed mechanisms for these reactions are elucidated with the help of quantum chemical calculations at the G2M level of theory. Reactions R1−R3 initially produce chemically activated intermediates interconnected by isomerization pathways on the extended [C_8H_9] potential energy surface. All kinetically important transformations of these isomeric C_8H_9 radicals are explicitly characterized and utilized in the construction of multichannel kinetic models for reactions R1−R3. Accurate thermochemistry is evaluated for the key intermediates from detailed conformational and isodesmic analyses. An examination of the G2M energetic parameters for reactions R1−R3 and for briefly revisited $C_6H_5 + C_2H_2$ and $C_6H_6 + H$ addition reactions reveals common theoretical deficiencies and suggests that the quality of theoretical predictions can be improved by small systematic corrections. Theoretical molecular and adjusted energetic parameters are used in a consistent way to calculate the total rate constants and product branching for reactions R1−R3 by weak collision master equation/RRKM analysis (addition channels) and transition state theory with Eckart tunneling corrections (abstraction channels). The available experimental kinetic data for reactions R1 and R2 is surveyed and found in good agreement with the best theoretical estimates.

I. Introduction

A better understanding of the mechanisms of hydrocarbon (HC) combustion and atmospheric degradation has been a major research initiative in the course of the last two decades.[1−3] The progress in this field, however, is critically dependent on the availability of reliable kinetic data for elementary reactions. In previous studies,[4−7] we reviewed available experimental data for reactions of benzene with some typical combustion radicals (e.g., R = H, CH_3, OH) and examined different theoretical approaches to the calculation of kinetic and thermodynamic parameters from the first principles. Kinetic data for reactions involving heavier aromatic hydrocarbons and radicals remains rather scarce. Thus, current models have to rely on the available data for prototypical reactions. Recently, we have employed our best methodologies to study the mechanism and kinetics of the phenyl radical reaction with acetylene,[8] a prototypical reaction of the molecular growth of polycyclic aromatic hydrocarbons (PAH). In this study, we will focus on reactions R1−R3 taking place on the [C_8H_9] potential energy surface:

$$C_6H_5 + C_2H_4 \rightarrow products \quad (R1)$$

$$C_2H_3 + C_6H_6 \rightarrow products \quad (R2)$$

$$H + C_6H_5C_2H_3 \rightarrow products \quad (R3)$$

These reactions involve important fuel components as well as radicals generated during HC combustion and pyrolysis. Reactions R1−R3 may also be considered prototypes of many

processes relevant to PAH formation. Among the key intermediates involved in reactions R1−R3 are the 1- and 2-phenylethyl radicals, which are produced in the pyrolysis and combustion of ethylbenzene and its α-substituted derivatives.[9] The 2-phenylethyl radical (**1**, Figure 1) is also generated during in vivo oxidation of a tranquilizing drug phenelzine (phenylethylhydrazine), and it is used as a model radical to study the metabolism of hydrazine derivatives as well as protein and DNA damage by C-centered radicals.[10] In turn, the 1-phenylethyl radical (**2**) is used in the chemistry of polymers as a mimetic compound for studying the selectivity of reactions of the growing polystyrene radical with different monomers.[11] Therefore, molecular and chemical properties of these radicals are of general interest.

Limited experimental kinetic data[12−14] are available for reactions R1 and R2 (see Table 1), which can be used to test the reliability of theoretical predictions. Stein and co-workers[12] used the very low pressure pyrolysis (VLPP) of C_6H_5NO, $C_6H_5SO_2C_2H_3$, and $Hg(C_2H_3)_2$ to generate phenyl and vinyl radicals and measured the rates of vinylation and phenylation of C_2H_2, C_2H_4, and C_6H_6 in a flow reactor connected to a quadrupole mass spectrometer. The H + $C_6H_5C_2H_3$ products were identified for both reactions R1 and R2 over the *T* range of 1000−1330 K. The corresponding vinylation (k_{R2}) and phenylation (k_{R1}) rate constants were determined relative to the assumed rate constants, $k_{R4} = 2.0 \times 10^{13}$ cm^3 mol^{-1} s^{-1} and $k_{R5} = 3.2 \times 10^{12}$ cm^3 mol^{-1} s^{-1}, for the following recombination reactions:

$$C_2H_3 + C_2H_3 \rightarrow H_2C{=}CHCH{=}CH_2 \quad (R4)$$

$$C_6H_5 + C_6H_5 \rightarrow C_6H_5C_6H_5 \quad (R5)$$
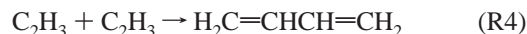
More recently, the high-*T* reactions of phenyl were studied by Heckmann et al.[15] in reflected shock waves. They reported
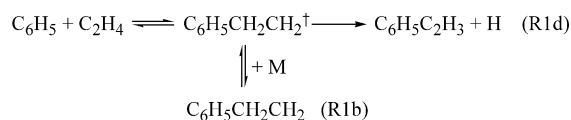
TABLE 1: Experimental Kinetic Data for the $C_6H_5 + C_2H_4$ and $C_2H_3 + C_6H_6$ Reactions

rate constant /cm^3 mol^{-1} s^{-1}	T /K	P /Torr	method	ref
$k_{R2} = 7.9 \times 10^{11} \exp(-3220/T)$	1000–1330	$(1-10) \times 10^{-3}$	VLPP/MS^a	12
$k_{R1} = 2.5 \times 10^{12} \exp(-3120/T)$	1000–1330	$(1-10) \times 10^{-3}$	VLPP/MS^a	12
$k_{R1} = 3.3 \times 10^{12} \exp(-3120/T)$	1000–1330	$(1-10) \times 10^{-3}$	reevaluation^b	
$k_{R1} = 7.2 \times 10^{11} \exp(-2250/T)$	297–523	20	CRDS	14

^{a} Relative rate measurement, assuming the reference rate constants $k_{R4} = 2.0 \times 10^{13}$ cm^3 mol^{-1} s^{-1}, $k_{R5} = 3.2 \times 10^{12}$ cm^3 mol^{-1} s^{-1}. ^{b} $k_{R1}^{new} = k_{R1}(k_{R5}^{new}/k_{R5})^{0.5}$, using $k_{R5}^{new} = 5.7 \times 10^{12}$ cm^3 mol^{-1} s^{-1} recommended by Heckmann et al.[15]

SCHEME 1

$$C_6H_5 + C_2H_4 \rightleftharpoons C_6H_5CH_2CH_2{}^\dagger \longrightarrow C_6H_5C_2H_3 + H \quad (R1d)$$

$$\big\Vert + M$$

$$C_6H_5CH_2CH_2 \quad (R1b)$$

a higher value of $k_{R5}(T = 1050-1450$ K$) = 5.7 \times 10^{12}$ cm^3 mol^{-1} s^{-1}, which we used to reevaluate the k_{R1} rate constant (see Table 1). Our conservative estimates[83] of the uncertainties in k_{R5} and k_{R4} amount to factors of 2 and 4, respectively. They propagate into factors of $2^{1/2}$ and 2 uncertainties in the absolute values of k_{R1} and k_{R2}, respectively. On top of that is the experimental error[12] of $\pm30\%$, resulting in factors of 2 and 2.6 combined uncertainties in the reevaluated high-T experimental values of k_{R1} and k_{R2}, respectively.

Preidel and Zellner[13] attempted to measure the phenyl radical kinetics by monitoring the continuous wave laser absorption signal at 488 nm. Its assignment to phenyl radical has not been confirmed in the later studies.[21,22] They have also concluded that the rate constants determined by this technique are unreliable.

The only direct measurement of the total rate of reaction R1 was reported by Yu and Lin,[14] using the cavity ring-down spectrometry (CRDS) technique. They also gave a theoretical interpretation of their low-T experimental results and the high-T kinetic data of Stein et al.[12] in terms of RRKM theory (Scheme 1), employing approximate energetic and molecular parameters.

The experimental studies described above provided important benchmark values of the total rate constants k_{R1} and k_{R2}, but to the best of our knowledge no attempt was made to characterize the intermediates or products of reactions R1 and R2 other than H + $C_6H_5C_2H_3$. For the reverse reaction R3 of styrene with H-atoms, neither the rate constant nor product branching have been measured or calculated. Our goal in the present study is to provide a theoretical description of the mechanism and kinetics of reactions R1–R3. All three reactions initially produce the C_8H_9 chemically activated radicals that are interconnected by isomerization pathways on the extended [C_8H_9] potential energy surface (PES). Following the description of computational procedures, we will present the extended PES for reactions R1–R3 calculated with chemical accuracy and the truncated kinetic models for individual reactions, including all kinetically important branches. Then the effective total and branching rate constants will be determined through a comprehensive RRKM-ME analysis[23–25] of the evolution of the chemically activated C_8H_9 radicals. The RRKM-ME analysis here denotes a procedure consisting of the Rice–Ramsperger–Kassel–Marcus calculation of the microcanonical rate constants, $k(E)$, for all elementary reactions included in the kinetic model, coupling of these $k(E)$s with the collisional energy transfer rates by means of a time-dependent 1-D (E-resolved) master equation (ME), and analysis of the evolution of reactive intermediates by solving the ME for each set of experimental conditions.

II. Computational Methods

II.1. Electronic Structure Calculations. The Gaussian 03[26] and MOLPRO 2002[27] program packages were used for ab initio and density functional theory calculations. The molecular and energetic parameters for all species relevant to reactions R1–R3 were calculated in the framework of the G2M composite method.[28] The present implementation is slightly different from the original versions of Mebel et al.,[28] as described below.

The equilibrium geometries of the reactants, products, and intermediates were optimized with the B3LYP[29] density functional at the 6-311++G(d,p) level,[30] using analytic gradients and force constants.[31] Tight convergence criteria were reinforced in both geometry and electronic wave function optimizations. This method is renowned for providing good quality molecular structures and vibrational frequencies at a moderate computational cost.[32] The calculated and available experimental[33] vibrational data for ethylene, benzene, styrene, vinyl and phenyl radicals are listed in the Supporting Information. From the present comparisons and our earlier examinations, the B3LYP harmonic frequencies of various hydrocarbons and their radicals are on average ~2–3% higher than the experimental fundamentals. Scaling factors of the same magnitude have been proposed.[34] We used calculated frequencies without any adjustments mainly because of their small deviations from the available experimental data and the negligible effect of frequency scaling on the calculated thermodynamic functions and kinetic parameters.

The performance of the B3LYP method for the optimization of transition states is more difficult to assess, but its failures to predict accurate barriers for reactions involving loose transition states are well-documented. In such cases, not only energies, but the geometric parameters, may be inaccurate[35] (typically, the B3LYP-optimized transition states are too loose and the barriers are too small, up to the point when they disappear at very long separations). We attempted to cure this deficiency with a modified three-step optimization procedure: (1) the minimum energy path (MEP) was optimized on the B3LYP PES either by following an intrinsic reaction coordinate[36] or by a relaxed scan along a certain internal coordinate (i.e., a bond stretching for association reactions); (2) the refined TS was located as the point on the MEP where the RCCSD(T)/6-311G(d,p) energy was at its maximum; (3) projected B3LYP vibrational frequencies were calculated at the refined TS. In the following, the acronym B3LYP will refer to the standard optimization by the B3LYP/6-311++G(d,p) method, whereas the modified procedure will be abbreviated as RCCmax. The latter is analogous to the IRCMax calculation[37] in Gaussian 03, except here the higher-level single-point energy calculations were carried out in MOLPRO 2002. The IRCMax approach has been recently employed by Saeys et al.[38] to obtain high-level (CBS-QB3) TS geometries along the less expensive B3LYP/6-311G(d,p) reaction paths. The IRCMax geometries have shown systematic improvement over the B3LYP data for radical addition reactions similar to the ones studied here.

Quantum Chemical/RRKM-ME Computational Study

J. Phys. Chem. A, Vol. 108, No. 45, 2004 **9699**

To obtain chemically accurate energetic parameters, the (R/U)CCSD(T)/6-311+G(3df,2p) electronic energies were approximated from a series of (R/U)CCSD(T), (P/U)MP4(SDTQ), and (R/U)MP2 single-point calculations on the lower-level optimized structures. In the above notations, methods with prefixes (R), (P), and (U) differ only for open-shell systems. Specifically, (R)CCSD(T)[39] here denotes a partially spin-adapted open-shell coupled cluster singles and doubles theory augmented with a perturbation correction for triple excitations (MOLPRO keyword RHF-RCCSD(T)); (P)MP4[40] is an approximate spin-projected MP4(SDTQ) energy after annihilation of $s + 1$ to $s + 4$ spin states; (R)MP2[41] is a spin-restricted open-shell MP2 (Gaussian keyword ROMP2). Our most accurate model is defined by the following equations:

$$E[G2M(RCC5)] = E[(R)CCSD(T)/6\text{-}311G(d,p)] + \Delta E(+3df2p) + \text{ZPE} \quad \text{(I)}$$

$$\Delta E(+3df2p) = E[(R)MP2/6\text{-}311+G(3df,2p)] - E[(R)MP2/6\text{-}311G(d,p)] \quad \text{(II-R)}$$

where the zero-point vibrational energy (ZPE) is calculated at the B3LYP/6-311++G(d,p) level. A less computationally demanding G2M(RCC6) version has been considered also

$$E[G2M(RCC6)] = E[(P)MP4/6\text{-}311G(d,p)] + \Delta E(RCC) + \Delta E(+3df2p) + \text{ZPE} \quad \text{(III-R)}$$

$$\Delta E(RCC) = E[(R)CCSD(T)/6\text{-}31G(d,p)] - E[(P)MP4/6\text{-}31G(d,p)] \quad \text{(IV-R)}$$

Compared to the original G2M schemes of Mebel et al.,[28] the basis set extension term is now evaluated by the (R)MP2 method, instead of (U)MP2, and the empirical higher-level corrections (HLCs) are omitted in the present versions. Replacing (U)MP2 with (R)MP2 helps to cure possible deficiencies of the former method due to high spin contamination in the UHF reference wave functions for aromatic and delocalized radicals. To further illustrate the differences between the spin-restricted and spin-unrestricted approaches, selected energies have also been calculated by the G2M(UCC6) model, which approximates the (U)CCSD(T)/6-311+G(3df,2p) level of theory:

$$E[G2M(UCC6)] = E[(P)MP4/6\text{-}311G(d,p)] + \Delta E(UCC) + \Delta E(+3df2p) + \text{ZPE} \quad \text{(III-U)}$$

$$\Delta E(+3df2p) = E[(U)MP2/6\text{-}311+G(3df,2p)] - E[(U)MP2/6\text{-}311G(d,p)] \quad \text{(II-U)}$$

$$\Delta E(UCC) = E[(U)CCSD(T)/6\text{-}31G(d,p)] - E[(P)MP4/6\text{-}31G(d,p)] \quad \text{(IV-U)}$$

We note that individual HLCs should be derived for each altered G2M scheme before it can be used for nonisogyric reactions. However, all reactions considered in this study are isogyric (with a conserved number of electron pairs), in which case the HLCs cancel out in all relative energies.

II.2. Rate Constant Calculations. Statistical theory rate constant calculations were performed with the ChemRate program[42] available from NIST. Molecular parameters listed in the Supporting Information were employed for the partition function, sum, and density of states computations followed by transition state theory (TST) calculations of elementary rate constants and RRKM calculations of microscopic rate constants:

$$k(E) = \frac{m^*}{m} \frac{N^*_{QM}(E)}{h\rho(E)} \quad \text{(V)}$$

where m^*/m is the path degeneracy due to optical isomers, $\rho(E)$ is the density of states of the active intermediate, $N^*_{QM}(E)$ is the sum of states of the transition state, including the effect of tunneling:[43]

$$N^*_{QM}(E) = \sum_j P(E - \epsilon^*_j) \quad \text{(VI)}$$

Summation is taken over all vibrational energy levels of the transition state; ϵ^*_j denotes the energy of level j; $P(E_1)$ is the one-dimensional (1-D) tunneling probability for a level with energy E_1 in the reaction coordinate. The E_1 is negative for levels with energy insufficient to overcome the barrier, so these levels contribute to the reaction rate only by tunneling. In the classical limit, $P(E_1)$ becomes a step-function:

$$P(E_1 < 0) \rightarrow H(E_1 < 0) = 0, \quad P(E_1 > 0) \rightarrow H(E_1 > 0) = 1 \quad \text{(VII)}$$

Assuming an unsymmetric Eckart form of the 1-D reaction profile, $P(E_1)$ can be calculated analytically[5,44] as a function of the reaction barriers (in forward and reverse directions), imaginary frequency, and energy E_1. At the high-pressure limit, the Eckart tunneling correction to the TST rate constant is expressed simply as a T-dependent factor calculated by integration of the energy specific probability $P(E_1)$ over the Maxwell–Boltzmann distribution.

Many intermediates and transition states involved in reactions R1–R3 have weakly hindered torsional motions among their internal degrees of freedom. The hindered rotor treatment[45] was applied to evaluate their contributions to the statistical functions. The reduced moments of inertia (I_R) were calculated according to Pitzer and Gwinn,[46] including a correction for rotor–rotor coupling. Torsional potentials were approximated as one-dimensional i-fold potentials of the form

$$V(\tau) = 0.5V_i(1 - \cos(i\tau)) \quad \text{(VIII)}$$

This form cannot accurately reproduce asymmetric potentials, which may require additional Fourier terms to be included. In the worst case of an asymmetric rotor relevant to this study, the symmetric hindered rotor treatment overestimates the low-T partition function by up to a factor of 2. Comparable errors are expected in the calculated rate constants due to uncertainties in the torsional barriers (V_i). For stable intermediates, the torsional barriers (V_i) were obtained from detailed conformational analyses using the B3LYP density functional. For transition states, the V_i's were either assumed to be the same as in the reactants or estimated from torsional frequencies (ν/cm^{-1}), using the following relation:

$$V_i \approx 8\pi^2 I_R N_A c^2 \nu^2 / i^2 \quad \text{(IX)}$$

To calculate the effective bimolecular rate constants and product distributions, we have to analyze on a microcanonical level the interplay of chemical activation, isomerization, and decomposition channels for the present multiple quantum well systems and also properly account for the energy transfer effects. A rigorous way of predicting the kinetics of such systems is to solve the time-dependent master equation (ME) which denotes a set of coupled integro–differential equations of motion for populations of specific
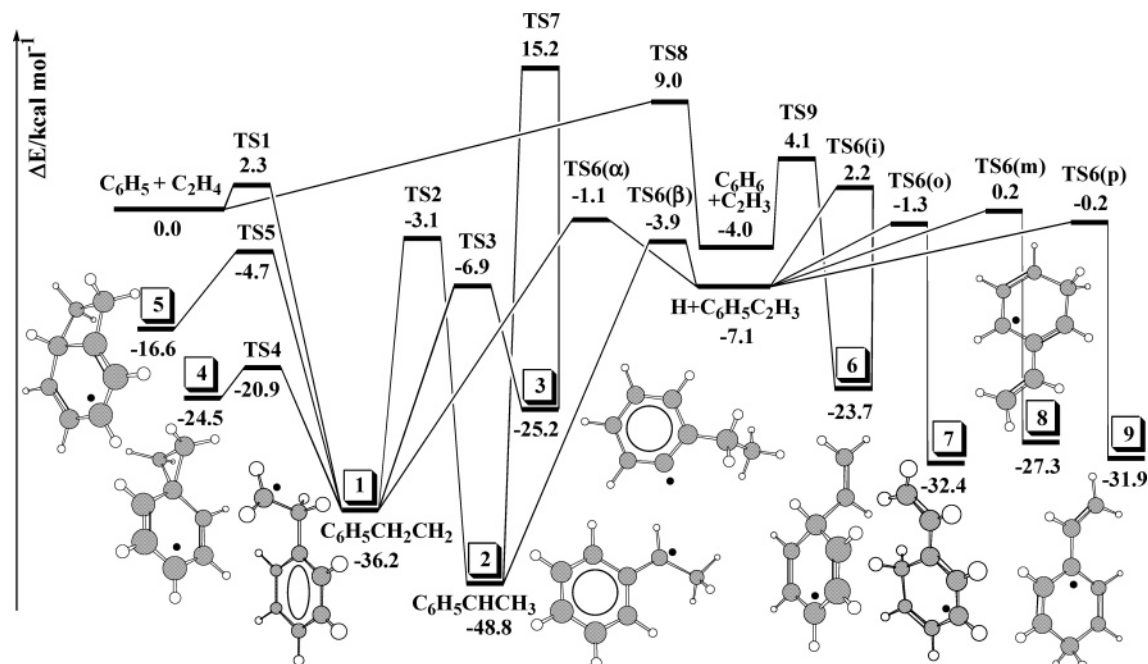
Figure 1. Potential energy diagram for reactions R1−R3. ZPE-corrected energies (kcal/mol) relative to $C_6H_5 + C_2H_4$ are calculated by the G2M(RCC5) method.

energy levels of the reactive intermediates:

$$\frac{\partial g_i(E,t)}{\partial t} = \omega \int_{E_{oi}}^{\infty} P_i(E,E')g_i(E',t)\,dE' - \omega g_i(E,t) - k_i(E)g_i(E) + r(E,t) \quad (X)$$

where $g_i(E,t)$ is the population of energy level E in well i at time t, ω is the collision frequency, E_{0i} is the ground state energy of well i, $P_i(E,E')$ is the transition probability for a molecule in well i with energy E' to go on collision to another state in the same well with energy E, $k_i(E)$ is the total rate constant of decay via all isomerization and decomposition channels open from well i at energy E, $r(E,t)$ is the rate of formation of species i with energy E from the chemical activation and isomerization channels.

For each of the present truncated kinetic models of reactions R1−R3, the single chemical activation channel provides a steady supply of reactive intermediates from bimolecular reactants. We assume that both reactants have Boltzmann distribution functions. Since we are only interested in the initial product branching, an "infinite sink" approximation is used for bimolecular product channels. All energy transfer acts are induced by weak molecular collisions of the chemically activated intermediates with bath gas and the energy transfer probabilities are given by the standard "exponential-down" model[23] with an empirical value of 400 cm^{-1} for $<\Delta E>_{\text{down}}$ (average energy loss per collision). The frequency of collisions was derived from the Lennard-Jones (L-J) parameters of Ar ($\sigma(\text{Ar}) = 3.54$ Å, $\epsilon/k_B(\text{Ar}) = 93.3$ K)[47] and C_8H_9 ($\sigma(C_8H_9) = 5.70$ Å, $\epsilon/k_B(C_8H_9) = 550$ K). The latter values are obtained from an empirical relationship between the L-J parameters and molecular weight established for a series of aromatic hydrocarbons,[48] and they are very similar to the L-J parameters for styrene estimated from its boiling point.[48] The ME was solved in a matrix form (for an array of discrete states ϵ_j, each with width δE, and energy-dependent functions represented by vectors) with a method based on the Householder and QR algorithms[49] for tridiagonalization and determination of eigenvalues and eigenfunctions. The energy bin size $\delta E = 100$ cm^{-1} and a maximum energy $E_{\text{max}} = 250$

kcal/mol were used in the ME computations to ensure the convergence at high T. Additional details about the implementation of the time-dependent weak collision ME/RRKM analysis in ChemRate are available from a series of publications by Tsang and co-workers.[50]

III. Results and Discussion

III.1. Potential Energy Surface. The global PES for reactions R1−R3 is schematically shown in Figure 1. The relative energies given in this figure are calculated by the G2M(RCC5) method, the highest level of theory employed in this study. The energetic parameters calculated at other theoretical levels are given in the Supporting Information (Tables S4−S8). The molecular parameters of the reactants, products, key intermediates, and transition states are also summarized in the Supporting Information (Tables S1, S2). First, we begin with a detailed description of the pathways involved in the reaction of phenyl with ethylene (R1). Then we will present our results for all branching channels of the H-atom addition to styrene, and finally, comment on the mechanism of the vinyl radical reaction with benzene (R3).

III.1.A. $C_6H_5 + C_2H_4$ Reaction. The C_6H_5 radical can attack ethylene either at the H or C sites. The first pathway leads to the H-abstraction via TS8:

$$C_6H_5 + C_2H_4 \rightarrow C_6H_6 + C_2H_3 \quad (R1a)$$
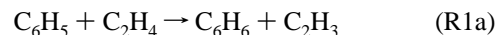
This channel has a relatively high barrier (∼9.0 kcal/mol); therefore, it is less important than the second pathway, electrophilic addition to the double bond via TS1:
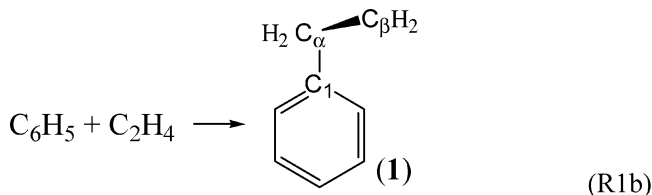
Both TS1 and TS8 have been optimized using the RCCmax
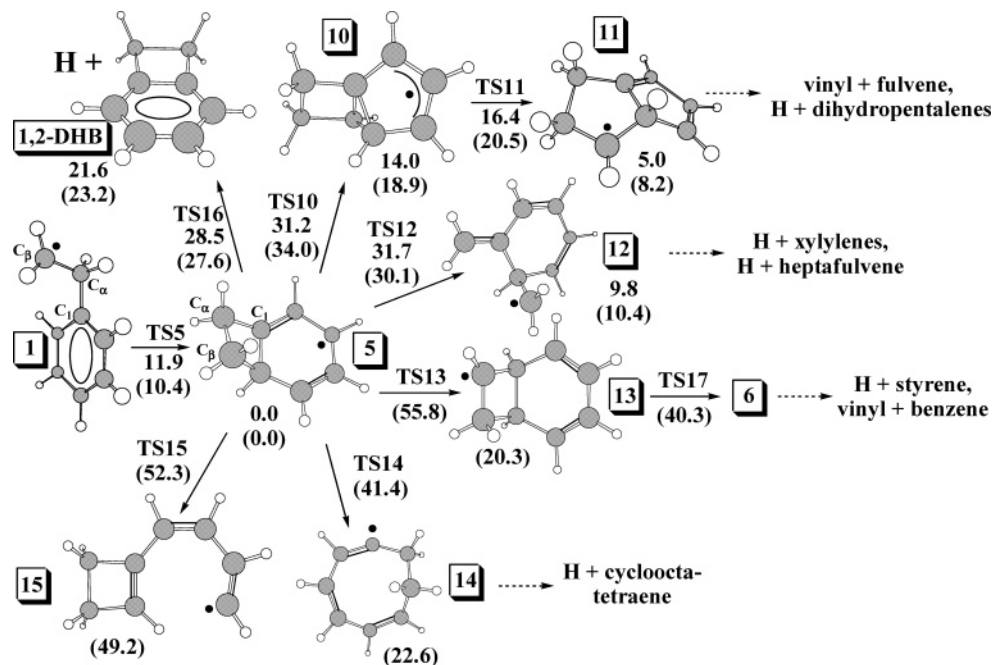
Figure 2. Potential energy diagram for the bicyclic branch of reaction R1. ZPE-corrected energies (kcal/mol) relative to $C_6H_5 + C_2H_4$ are calculated by the G2M(RCC6) and B3LYP/6-311++G(d,p) (values in parentheses) methods.

procedure. The geometry of TS8 turned out to be the same as the one optimized by the B3LYP method. The low-barrier TS1 is more sensitive to the optimization method. The TS1//RCCmax is located at the C_1-C_α separation of 2.33 Å, which is 0.1 Å shorter than the C_1-C_α bond in the TS1//B3LYP. The G2M(RCC5) barrier for reaction R1b changes from 2.1 to 2.3 kcal/mol when the B3LYP-optimized structure of TS1 is refined by the RCCmax procedure.

Reaction R1b initially produces chemically activated 2-phenylethyl radicals (**1**), which have sufficient energy to undergo several isomerization and decomposition reactions. The molecular structure and conformational behavior of radical **1** will be discussed in the next section. For now, we will focus on its chemistry. We have considered radical eliminations (β-scissions), H-migrations, and cyclizations (intramolecular radical additions) as the most viable unimolecular transformations on the [C_8H_9] PES, because these types of reactions were found to be important in our recent theoretical investigation of the [C_8H_7] PES.[8]

Let us begin with possible cyclization reactions of **1**. Intramolecular additions of the side chain radical at the meta- and para-positions of the C_6 ring are expected to be strongly unfavorable, because the products are very strained bicyclic radicals, not stabilized by conjugation. We have recently examined similar cyclization processes of the 2-phenylvinyl radical and found that they can be safely neglected.[8] By analogy, only ipso- and ortho-cyclizations need to be considered for radical **1**.

The intramolecular addition of the side chain radical at the ipso-position of the aromatic ring is the most facile rearrangement of **1**. The spiro[2,5]octadienyl radical (**4**) produced by ipso-cyclization of **1** is very short-lived and appears as a shallow minimum on the reaction profile for the 1,2-migration of phenyl in **1**:
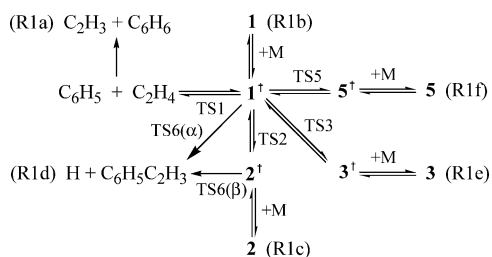

(R6)
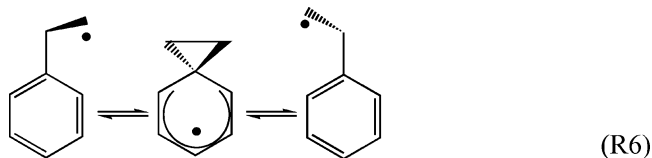
This process, also known as the neophyl rearrangement, has been studied both experimentally[51] and theoretically.[52] Corrected to standard conditions, the G2M(RCC5) activation energy of the **4** to **1** rearrangement is 3.5 kcal/mol. It is in reasonable agreement with the DFT estimate of Asensio and Dannenberg[52] (4.0 kcal/mol) and the experimental value of Effio et al.[51c] (2.8 ± 0.4 kcal/mol) estimated from the limited kinetic data measured in solution by laser photolysis with optical and ESR detection methods.

The ortho-cyclization of **1** yields bicyclo[4.2.0]octa-2,4-dien-1-yl radical (**5**, Figure 2). The **1** to **5** rearrangement has a relatively high barrier of 31.5 kcal/mol, because it creates strained C_6 and C_4 rings which are fused in such a manner as to force a pyramidal (instead of the optimal planar) geometry at the vinylic C_1 atom. Nevertheless, TS5 is accessible by the chemically activated radical **1**. Therefore, we have also explored various isomerization and decomposition pathways originating from **5**.

Depicted in Figure 2 are the most conceivable rearrangements of radical **5**, which link it to various C_8H_9 isomers (**10**−**15**) with a different structure of the carbon backbone. Radicals **10**−**15** are potentially important intermediates for such reactions as vinyl + fulvene, H + C_8H_8 (various isomers), and others. However, they are separated from **5** by high barriers, inaccessible from the $C_6H_5 + C_2H_4$ reactants. The rearrangement of **13** to **6** and many other isomerizations involving these radicals have been studied by semiempirical (AM1, PM3) and molecular mechanics methods.[53] Although the energetic parameters predicted by those methods are only semiquantitatively accurate, none of the secondary isomerization channels of radicals **6** and **13** appear to be important for the mechanism of reactions R1−R3. Hence, the only kinetically important transformation of **5** is the ring opening via TS5 that brings it back to **1**.

Besides cyclizations, radical **1** can undergo 1,2 and 1,4 H-migrations, involving the neighboring C−H bonds at the α- and ortho-positions, respectively. Migration of the α-hydrogen is exothermic and leads to the 1-phenylethyl radical (**2**), a benzyl-type radical stabilized by π-conjugation. On the other hand, the 1,4 H-migration in **1**, leading to the phenyl-type radical **3**, is endothermic, because the aromatic ortho-(C−H) bond is
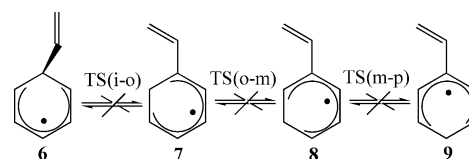
SCHEME 2

(R1a) $C_2H_3 + C_6H_6$ $\mathbf{1}$ (R1b)

$C_6H_5 + C_2H_4 \underset{TS1}{\overset{}{\rightleftharpoons}} \mathbf{1}^\dagger \underset{TS5}{\overset{}{\rightleftharpoons}} \mathbf{5}^\dagger \overset{+M}{\rightleftharpoons} \mathbf{5}$ (R1f)

(R1d) $H + C_6H_5C_2H_3 \underset{TS6(\beta)}{\overset{TS6(\alpha)}{\leftarrow}} \mathbf{2}^\dagger \qquad \mathbf{3}^\dagger \overset{+M}{\rightleftharpoons} \mathbf{3}$ (R1e)

$\mathbf{2}$ (R1c)

stronger than the aliphatic $C_\beta-H$ bond. The barriers for these H-migrations are relatively high, because they involve tight three- and five-center transition states (TS2 and TS3) with strongly distorted C−C−H angles, particularly TS2. But again, both transition states are accessible through reaction R1. This is not the case for TS7 that lies very high on the 1,3 H-migration pathway directly connecting **2** and **3**. Remarkably, the latter process is much more difficult than the 1,2 and 1,4 H-shifts described above. The possible reasons are that, unlike the five-center TS3, the four-center TS7 is considerably more strained, and, unlike in TS2, the unpaired electron in TS7 has to rotate inside the C_6-plane and break the conjugation with the aromatic ring before it achieves substantial overlap with the antibonding ortho-(C−H) orbital. The associated energetic expenses raise the energy of TS7 by more than 18 kcal/mol relative to that of TS2.

The only remaining kinetically important transformations of **1** and **2** are the H-eliminations (via TS6(α) and TS6(β), respectively). Both TS6(α) and TS6(β) have been optimized using the RCCmax procedure. The breaking $C_\alpha-H$ bond in TS6(α) is 1.85 Å long, which is ~0.15 Å shorter than the breaking $C_\beta-H$ bond in TS6(β). For comparison, the standard B3LYP optimization fails to predict the relatively small barrier for H-addition at the terminal C_β atom in styrene and locates TS6(α) at $r(C_\alpha-H) = 1.98$ Å. Although TS6(β) is easier to overcome than TS6(α), this channel is not directly accessible from **1** due to the relatively high barrier of 33 kcal/mol (TS2) separating **1** and **2**. An interesting question is whether the direct H-elimination from **1** is a more efficient styrene-producing pathway than a two-step sequence consisting of the 1,2 H-shift followed by the H-elimination from **2**. This question will be addressed later in this work.
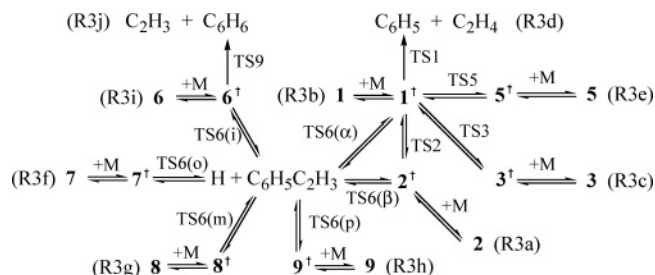
The mechanism that includes key pathways accessible by reaction R1 can be expressed by Scheme 2 which will be used as a basis for our rate constant calculations discussed later in this article. This scheme is based on a truncated version of the PES for reaction R1 featuring only six product channels and four intermediates.

The 1,2 phenyl-shift in **1** (R6) is omitted in Scheme 2, because it does not produce any new chemical species and, therefore, does not bear any kinetic consequences for reaction R1. In addition, the secondary reactions of radicals **5** and **3** have been excluded, because the associated barriers (TS7, TS10−TS16) are too high. Additional transformations that might be suggested for **3** include the 1,2 H-shift in the aromatic ring, 1,3 CH_3-shift, and benzyne production by β-scission of the C_1-C_α bond. These are all very unlikely possibilities. The 1,2 H-shift in **3** has been ruled out based on the expectation that the corresponding three-center transition state should be much higher in energy than TS2, since the aromatic C−H bond is much stronger than the benzylic C−H bond. The transition state for the 1,3 CH_3-migration in **3** was optimized by the B3LYP/6-311++G(d,p) method. As expected, the barrier for this shift (63 kcal/mol) is much higher than TS7, the barrier for the 1,3 H-shift in **3**.
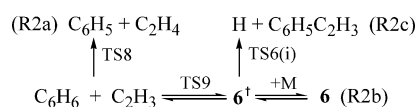
SCHEME 3

SCHEME 4

SCHEME 5

(R2a) $C_6H_5 + C_2H_4$ $H + C_6H_5C_2H_3$ (R2c)

$\uparrow$ TS8 $\uparrow$ TS6(i)

$C_6H_6 + C_2H_3 \underset{TS9}{\overset{}{\rightleftharpoons}} \mathbf{6}^\dagger \overset{+M}{\rightleftharpoons} \mathbf{6}$ (R2b)

Finally, formation of benzyne + C_2H_5 in reaction R1 can be neglected due to a very high endothermicity (> 40 kcal/mol).
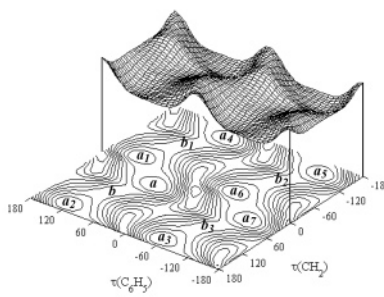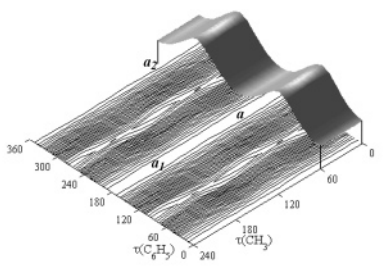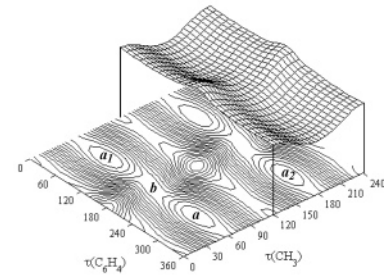
III.1.B. $H + C_6H_5C_2H_3$ Reaction. In addition to the pathways mentioned above in Scheme 2, the H-atom can also add to the aromatic ring in styrene. Overall, six distinct channels must be considered, namely, H α-, β-, ipso-, ortho-, meta-, and para-additions forming relatively stable radicals **1**, **2**, and **6**−**9**. As follows from the energies of TS6 shown in Figure 1, the β-addition pathway forming radical **2** is the most favorable. Other C_8H_9 isomers are initially produced by reaction R3 in the following order of preference: **6** < **8** < **9** < **1** < **7** < **2**. The associated barriers calculated by the G2M(RCC5)//RCCmax method range from 3.2 (TS6(β)) to 9.3 (TS6(i)) kcal/mol. As mentioned earlier, radicals **1** and **2** are separated by a relatively high barrier (TS2). The 1,2 H-shifts interconnecting radicals **6**−**9** (Scheme 3) have barriers that lie more than 18 kcal/mol higher than TS2, according to our DFT estimates. Therefore, wells **6**−**9** can be treated as uncoupled for kinetic applications.

In fact, the only kinetically important transformation of **7**−**9** is the elimination of H, reforming styrene. Only **6** may undergo the C_2H_3-elimination pathway via TS9 that leads to the new products, $C_2H_3 + C_6H_6$. The pathway connecting **6** to **1** via TS17, **13**, TS13, **5** and TS5 (see Figure 2) is not accessible by reaction R3, because the barrier (TS17) for the ortho-cyclization of **6** to **13** lies more than 30 kcal/mol above the H + $C_6H_5C_2H_3$. Since radicals **7**−**9** have a planar carbon backbone stabilized by π-conjugation, the barriers for their hypothetical cyclizations are expected to be even higher.

Overall, the truncated kinetic model of reaction R3 can be given by Scheme 4. The initial branching is between six channels, corresponding to H-addition at different sites in styrene. Upon inclusion of kinetically important transformations of radicals **1**, **2**, and **6**, the number of accessible product channels increases to 10 (R3a−R3j).

III.1.C. $C_2H_3 + C_6H_6$ Reaction. The PES constructed to describe the mechanism of reactions R1 and R3 (see Figure 1) contains all the pathways accessible from $C_2H_3 + C_6H_6$. The initial attack of the vinyl radical may target either the H or C atoms on benzene, leading either to the H-abstraction products (R2a) or to the addition (R2b) and C_2H_3-addition/H-elimination (R2c) products, as depicted in Scheme 5.

Quantum Chemical/RRKM-ME Computational Study

J. Phys. Chem. A, Vol. 108, No. 45, 2004 **9703**

TABLE 2: Conformational Analysis for Radicals 1−3

energetic profiles	conformation	sym	relative energy[a]		
			b	*c*	*d*
	1A	C_1	0.00	0.00	0.00
	1B	C_s	0.39	0.26	0.32
	TS(**1a↔1b**)	C_1	0.43	0.30	0.34
	TS(**1a₁↔1a**)	C_s	0.27	0.10	0.07
	TS(**1a₃↔1a**)	C_s	1.17	1.16	1.25
	Torsional Barriers (approximate description) $\tau(CH_2)$: V_2 = 0.34 kcal/mol $\tau(C_6H_5)$: V_2 = 1.25 kcal/mol				
	2A	C_s	0.00		0.00
	TS(**2a↔2a₁**)	C_s	0.15		0.21
	TS(**2a↔2a₂**)	C_s	12.9		12.6
	Torsional Barriers (approximate description) $\tau(CH_3)$: V_3 = 0.21 kcal/mol $\tau(C_6H_5)$: treated as an oscillator				
	3A	C_1	0.00		0.00
	3B	C_s	0.98		0.98
	TS(**3a↔3b**)	C_1	1.01		1.00
	TS(**3a₁↔3a**)	C_s	0.42		0.54
	TS(**3a₂↔3a**)	C_1	3.30		3.14
	Torsional Barriers (approximate description) $\tau(C_6H_4)$: V_2 = 1.00 kcal/mol $\tau(CH_3)$: V_3 = 3.14 kcal/mol				

[a] Energies are in kcal/mol and do not include the ZPE correction. [b] B3LYP/6-31G(d,p). [c] B3LYP/6-311G(d,p) from ref 54. [d] B3LYP/6-311++G(d,p).
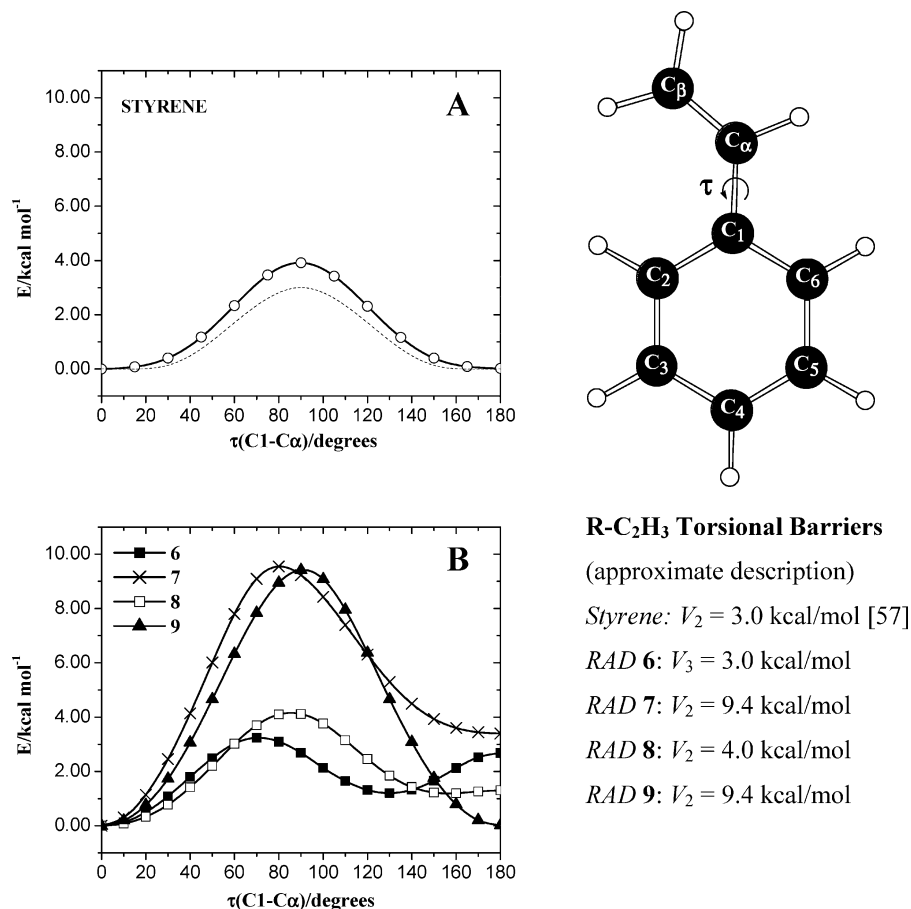
III.2. Conformational Analysis. The molecular structure of the key intermediates formed in reactions R1−R3 is flexible with respect to internal rotation about one or two noncyclic C−C bonds. In this section, we present the results of our detailed conformational analysis, which allowed us to identify the most stable conformations of radicals **1−3** and **6−9** and explicitly characterize the internal rotational pathways. A uniform atom numbering scheme given in Figure 3 for styrene will be used for radicals **1−3** and **6−9**, which have a similar structure of the carbon backbone.

Relaxed scans have been performed for radicals **1−3** on the B3LYP/6-31G(d,p) conformational energy surfaces spanned by two torsional coordinates, $\tau(C_1−C_\alpha)$ and $\tau(C_\alpha−C_\beta)$, describing the compound rotation of the CH_2 ($\tau(C_\alpha−C_\beta) = \tau(CH_2)$) and C_6H_5 ($\tau(C_1−C_\alpha) = \tau(C_6H_5)$) tops attached to the $C_\alpha H_2$ moiety in **1**, CH_3 ($\tau(C_\alpha−C_\beta) = \tau(CH_3)$) and C_6H_5 ($\tau(C_1−C_\alpha) = \tau(C_6H_5)$) tops attached to the $C_\alpha H$ moiety in **2**, CH_3 ($\tau(C_\alpha−C_\beta) = \tau(CH_3)$) and C_6H_4 ($\tau(C_1−C_\alpha) = \tau(C_6H_4)$) tops attached to the $C_\alpha H_2$ moiety in **3**. The contour line and perspective three-dimensional plots of the calculated conformational surfaces are given in Table 2. Stationary points (local minima and transition states) were reoptimized with the 6-311++G(d,p) basis set to

obtain more accurate torsional barriers, which are also listed in Table 2.

The lowest energy conformation of the 2-phenylethyl radical (conformation **1A**) is unsymmetric and 8-fold degenerate. Its molecular structure is shown in Figure 1. As follows from the energetic profile (see Table 2), any given minimum *a* is connected to three other degenerate forms (*a₁*, *a₂*, *a₃*) by three distinct minimum energy pathways (MEPs) that favor geared rotation of the CH_2 and C_6H_5 tops.

Following the pathway $a_4 \rightarrow a_1 \rightarrow a \rightarrow a_2$, one obtains the MEP for CH_2-rotation in **1**. The complete revolution of the CH_2 group about the $C_\alpha−C_\beta$ bond is facilitated by a synchronous restricted rotation (±30°) of the C_6H_5 group near the staggered position ($\tau(C_6H_5) = 90°$), that is, in and out of the plane orthogonal to the ($C_1−C_\alpha−C_\beta$) plane. Minima a_1 and *a* are separated by a very small barrier, TS(**1a₁↔1a**), where the CH_2 group lies in the ($C_1−C_\alpha−C_\beta$) molecular plane ($\tau(CH_2) = 0°$, eclipsed position) and the C_6H_5 is exactly perpendicular to it. On the MEP from *a* to *a₂*, a very shallow minimum *b* is found corresponding to the C_s-symmetric conformation **1B**, which is ~0.3 kcal/mol less stable than conformation **1A**. Conformation **1B** has both CH_2 and C_6H_5 groups in the staggered orientation

R-C₂H₃ Torsional Barriers

(approximate description)

Styrene: $V_2 = 3.0$ kcal/mol [57]

RAD 6: $V_3 = 3.0$ kcal/mol

RAD 7: $V_2 = 9.4$ kcal/mol

RAD 8: $V_2 = 4.0$ kcal/mol

RAD 9: $V_2 = 9.4$ kcal/mol

Figure 3. Internal rotational profiles and hindering barriers for styrene (Plot A) and radicals **6**−**9** (Plot B) calculated at the B3LYP/6-311++G(d,p) level of theory. The dashed line represents the CCSD(T)/extrap//CCD/-cc-pVDZ profile obtained in ref 57. Molecular structures ($\tau = 0°$ conformations) of radicals **6**−**9** are shown in Figure 1. Both the $\tau = 0°$ and $\tau = 180°$ conformations of radicals **6**−**9** have C_s molecular symmetry.

with respect to the $(C_1-C_\alpha-C_\beta)$ molecular plane ($\tau(CH_2) = \tau(C_6H_5) = 90°$). Energetically, the local minimum ***b*** essentially blends with two adjacent transition states, TS(**1a↔1b**) and TS(**1a₂↔1b**).

The MEP for C_6H_5-rotation passes through $a_3 \rightarrow a \rightarrow a_1 \rightarrow a_5$, in such a manner that the CH_2 group completes one revolution in-sync with the bulkier C_6H_5. The corresponding one-dimensional profile can be approximated by a 2-fold symmetric potential with a barrier, $V_2(C_6H_5) = 1.25$ kcal/mol. Neglecting small bumps and dips (TS(**1a₁↔1a**) and conformation **1B**, respectively) on the MEP for CH_2-rotation, the latter can be viewed also as a 2-fold symmetric potential with a barrier, $V_2(CH_2) = 0.3$ kcal/mol.

Internal rotation in **1** was previously studied by Van Speybroeck et al.[54] at the B3LYP/6-311G(d,p) level. Their one-dimensional rotational potentials are virtually identical to our results. The two-dimensional profile calculated in this study allows us to gain additional insights into the mechanism of internal rotation, in particular, the mutual coupling of internal rotors. In subsequent publications,[55] Van Speybroeck et al. have examined in further detail the implications of accurate treatment of coupled hindered rotation on the molecular partition functions and TST rate constants. This problem remains a topic of current research. Case studies available in the literature indicate that application of accurate coupling schemes typically leads to a moderate decrease of the partition functions compared to the uncoupled internal rotor approach. Nevertheless, the partition functions calculated by approximate uncoupled 1-D hindered rotor models remain closer to the accurate ones than those calculated within the harmonic oscillator approximation. We did not pursue the exact treatment of coupled internal rotations, because the errors associated with the approximate treatment of internal rotations in radical **1** and other species relevant to this study are expected to be minor.

We followed a similar procedure in order to analyze the conformational behavior of radicals **2** and **3**. The salient features of their conformational energy surfaces (see Table 2) are summarized below.

Internal rotations of the CH_3 and C_6H_5 groups in 1-phenylethyl (**2**) occur on two very different energetic scales. The CH_3-rotation is hindered by a vanishing barrier $V_3 = 0.2$ kcal/mol, whereas the C_6H_5-rotation is much more difficult due to the partial π-character of the exocyclic C_1-C_α bond. The predicted barrier, $V_2 = 12.6$ kcal/mol, is in close agreement with the experimental value, 13.4 ± 1.0 kcal/mol,[56] determined by ESR spectroscopy. Both harmonic oscillator and hindered rotor treatments are acceptable for calculating the partition function of the C_6H_5-torsional motion in **2**.

Similar to radical **1**, 2-ethylphenyl (**3**) radical has single C_1-C_α and $C_\alpha-C_\beta$ bonds about which the internal rotation is relatively facile. However, the topography of its conformational potential is more straightforward, because the MEPs for CH_3 and C_6H_4-rotations in 2-ethylphenyl radical (**3**) display virtually no mixing of the two motions: the CH_3 group is balancing close to its equilibrium orientation as the C_6H_4 group rotates about the C_1-C_α bond, and vice versa, the aromatic ring maintains staggered orientation relative to the $(C_1-C_\alpha-C_\beta)$ plane during the hindered rotation of the CH_3 group ($V_3 = 3.1$ kcal/mol). On the MEP for C_6H_4-rotation, a very shallow local minimum

Quantum Chemical/RRKM-ME Computational Study

J. Phys. Chem. A, Vol. 108, No. 45, 2004 **9705**

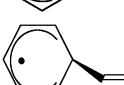**TABLE 3: Thermochemical Parameters of Selected Molecules and Radicals Relevant to This Study**
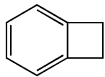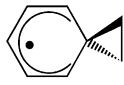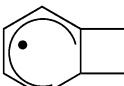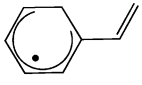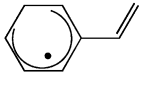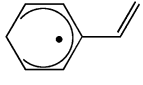
species	formula	$\Delta_fH°_0$, kcal mol^{-1}	$S°_{298}$, cal mol^{-1} K^{-1}	$\Delta_fH°_{298}$, kcal mol^{-1}	ref
Hydrogen	H	51.63	27.42	52.10	[33,58,59]
Methane	CH$_4$	-15.9±0.1	44.5	-17.8±0.1	[33,58,59]
Vinyl	C$_2$H$_3$	72.1±0.7	55.9[a]	71.1±0.7	[64,65]
		71.8±1.0			[72]
Ethylene	C$_2$H$_4$	14.6±0.1	52.4	12.5±0.1	[33,58,59]
Ethyl	C$_2$H$_5$	31.5±0.5[b]	58.9[b]	28.9±0.4	[60]
			59.0	28.9±0.4	[61]
				28.8±0.6	[62]
		31.4±0.5	59.2	28.8±0.5	[63]
Ethane	C$_2$H$_6$	-16.3±0.1	54.8	-20.1±0.1	[33,58,59]
Propane	C$_3$H$_8$	-19.7±0.1	64.6	-25.0±0.1	[33,58,59]
Phenyl	C$_6$H$_5$	83.7±0.6	68.9[a]	80.6±0.6	[64,66]
Benzene	C$_6$H$_6$	24.0±0.1	64.3	19.8±0.1	[33,58,59]
Cyclohexa-2,4-dienyl	C$_6$H$_7$	54.3±2.0	72.0[a]	49.5±2.0	[6]
Benzyl	C$_6$H$_5$CH$_2$	54.1±0.6	75.2[a]	49.7±0.6	[67]
		54.5±1.2		50.2±1.2	[68]
		54.7±1.0		50.3±1.0	[69]
				48.5±1.4	[70]
				49.7±1.2	[71]
		53.8±1.0			[72]
Toluene	C$_6$H$_5$CH$_3$	17.5±0.2	76.7	12.0±0.2	[33,58,59]
Styrene	C$_6$H$_5$C$_2$H$_3$	40.3±0.3	82.5	35.1±0.3	[33,59]
1,2-Dihydroben zocyclobutene		[51.7]	77.5[a]	[46.0]	P.w.[c]
1,2-DHB				47.7±0.2	[59]
2-Phenylethyl	C$_6$H$_5$CH$_2$CH$_2$ (**1**)	62.1±1.8	89.2[a]	56.4±1.8	P.w.[c]
		61.3	89.4	55.6	[58]
				54.5	[73]
1-Phenylethyl	C$_6$H$_5$CHCH$_3$ (**2**)	48.0±1.8	87.1[a]	42.0±1.8	P.w.[c]
		46.2	85.1	40.4	[58]
				40.8±1.3	[71]
				41.9	[75]
2-Ethylphenyl	o-C$_6$H$_4$C$_2$H$_5$ (**3**)	72.7±1.8	88.8[a]	66.8±1.8	P.w.[c]
				66.8	[74]
Spiro[2.5]octa-4,7-dien-6-yl	(**4**)	[73.8]	80.5[a]	[67.5]	P.w.[c]
Bicyclo[4.2.0] octa-2,4-dien-1-yl	(**5**)	[81.7]	80.5[a]	[75.2]	P.w.[c]
6-vinylcyclo hexa-2,4-dienyl	(**6**)	73.9±3.4	87.9[a]	68.0±3.4	P.w.[c]

TABLE 3 (Continued)

species	formula	$\Delta_f H°_0$, kcal mol^{-1}	$S°_{298}$, cal mol^{-1} K^{-1}	$\Delta_f H°_{298}$, kcal mol^{-1}	ref
1-vinylcyclohexa-2,4-dienyl (7)		65.2±3.4	85.2[a]	59.2±3.4	P.w.[c]
3-vinylcyclohexa-2,4-dienyl (8)		70.3±3.4	86.7[a]	64.4±3.4	P.w.[c]
2-vinylcyclohexa-2,4-dienyl (9)		65.7±3.4	83.9[a]	59.7±3.4	P.w.[c]

[a] Based on the B3LYP/6-311++G(d,p) molecular parameters. [b] Entropy and thermal correction are taken from ref 58. [c] Isodesmic enthalpies of formation from the present work; enthalpies in square brackets are calculated from the $\Delta_f H°_0(C_6H_5)$, $\Delta_f H°_0(C_2H_4)$, and G2M(RCC5) relative energies shown in Figure 1.
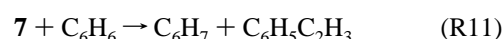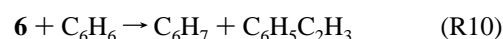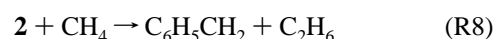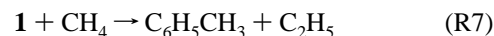
(conformation **3B**) is found when the C_6H_4 ring is rotating through the ($C_1-C_\alpha-C_\beta$) molecular plane and its ortho-hydrogen is pointing toward the CH_3 group. To a good approximation, conformation **3B** may be regarded as the C_6H_4-torsional barrier. Then the corresponding torsional potential is 2-fold degenerate with a barrier $V_2 = 1.0$ kcal/mol, but with the symmetry number equal to 1, which accounts for structural inequivalence of the degenerate minima a and a_1 (they are, in fact, two enantiomeric forms of radical **3**).

The internal rotational profiles for radicals **6**−**9** calculated by the B3LYP/6-311++G(d,p) method are shown in Figure 3B. The $C_\alpha-C_\beta$ bond in radicals **6**−**9** retains a strong double character. Therefore, we have only considered internal rotation of the C_2H_3 group about the C_1-C_α bond. As a benchmark, we have also included in Figure 3A the torsional potential of styrene, a precursor of radicals **6**−**9** via reaction R3.

The molecular structure of styrene has been reviewed recently by Sancho-Garcia and Perez-Jimenez.[57] Their final form of the classical torsional potential (dashed line in Figure 3A) was calculated at the CCSD(T) level extrapolated to the complete basis set; it was also corroborated by the available spectroscopic data. This potential features a barrier for internal rotation $V_2 = 3.0$ kcal/mol, which separates two quasi-planar minima stabilized by π-conjugation (barrier to planarity is less than 0.01 kcal/mol). The B3LYP potential is very similar to the benchmark CCSD(T) potential, but it slightly overestimates the torsional barrier.

Addition of the H-atom to styrene at the ortho-, meta- and para-positions preserves conjugation between the $C_\alpha-C_\beta$ double bond and π-electrons of the ring. In fact, the double character of the C_1-C_α bond becomes even stronger than in styrene, especially in radicals **7** and **9**, which is reflected in the increased torsional barriers given in Figure 3. On the other hand, in the absence of π-conjugation with the $C_\alpha-C_\beta$ double bond, the shape of the C_2H_3-torsional potential in radical **6** is determined by steric factors, primarily by the repulsive interactions of the $C_\alpha-H$ bond with the ipso- and ortho-(C−H) bonds. Three minima on the torsional potential of radical **6** have the $C_\alpha-H$ bond in the anti-periplanar position relative to either the ipso-(C−H) bond (global minimum shown in Figure 1) or ortho-(C−H) bonds (two enantiomeric local minima). Accordingly, the barriers correspond to the syn-periplanar conformations, where the repulsions between neighboring C−H bonds are maximized. Internal rotation in **6** can be approximately described by a 3-fold potential with a barrier $V_3 = 3.0$ kcal/mol and a symmetry number $n = 1$.

III.3. Isodesmic Reaction Analysis. Table 3 summarizes the thermochemistry of various species relevant to this study. The enthalpies of formation of the isomeric C_8H_9 radicals involved in reactions R1−R3 are not well-established. One way to estimate them is to combine the calculated relative energies from Figure 1 with the experimental enthalpies of formation of C_2H_4 and C_6H_5. Alternatively, more reliable estimates can be obtained from the isodesmic reaction analysis. We derived enthalpies of formation of the key intermediates of reactions R1−R3 through the following isodesmic reactions:

$$1 + CH_4 \rightarrow C_6H_5CH_3 + C_2H_5 \qquad (R7)$$

$$2 + CH_4 \rightarrow C_6H_5CH_2 + C_2H_6 \qquad (R8)$$

$$3 + CH_4 \rightarrow C_6H_5 + C_3H_8 \qquad (R9)$$

$$6 + C_6H_6 \rightarrow C_6H_7 + C_6H_5C_2H_3 \qquad (R10)$$

$$7 + C_6H_6 \rightarrow C_6H_7 + C_6H_5C_2H_3 \qquad (R11)$$

$$8 + C_6H_6 \rightarrow C_6H_7 + C_6H_5C_2H_3 \qquad (R12)$$

$$9 + C_6H_6 \rightarrow C_6H_7 + C_6H_5C_2H_3 \qquad (R13)$$
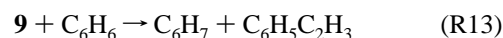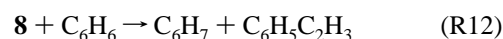
These hypothetical reactions contain similar types of bonds and radical systems in the reactants and products. As a result, different theoretical methods give very consistent predictions of the enthalpies of reactions R7−R13 by taking advantage of error cancellation. The values calculated at various levels of theory are collected in the Supporting Information (Table S3). At the highest G2M(RCC5) level of theory employed, we obtain $\Delta_{R7}H°_0 = 2.8 \pm 1.0$ kcal/mol, $\Delta_{R8}H°_0 = 5.7 \pm 1.0$ kcal/mol, $\Delta_{R9}H°_0 = 7.2 \pm 1.0$ kcal/mol, $\Delta_{R10}H°_0 = -3.3 \pm 1.0$ kcal/mol, $\Delta_{R11}H°_0 = 5.4 \pm 1.0$ kcal/mol, $\Delta_{R12}H°_0 = 0.3 \pm 1.0$ kcal/mol, and $\Delta_{R13}H°_0 = 4.9 \pm 1.0$ kcal/mol, where an assumed theoretical uncertainty of 1.0 kcal/mol has been included.

Then the isodesmic enthalpies of formation for radicals **1**−**3** and **6**−**9** can be derived from the theoretical enthalpies of reactions R7−R13 and experimental enthalpies of formation of other species involved in these reactions. The auxiliary thermochemical data for hydrocarbons is readily available from the TRC[58] and NIST[33,59] compilations (see Table 3). The enthalpies of formation for vinyl, ethyl, phenyl, cyclohexadienyl (C_6H_7), and benzyl radicals have been revised repeatedly. However, recent determinations of the $\Delta_f H°_{298}(C_2H_5)$ made by different experimental techniques[60−62] agree very well with each other

Quantum Chemical/RRKM-ME Computational Study

J. Phys. Chem. A, Vol. 108, No. 45, 2004 **9707**

TABLE 4: Enthalpies of Reactions (0 K, kcal/mol) Calculated Directly and Derived from Isodesmic Reaction Analysis[a,b]

	B3LYP		G2M(UCC6)		G2M(RCC6)		G2M(RCC5)		
enthalpy[c]	direct	isodesmic	direct	isodesmic	direct	isodesmic	direct	isodesmic	best value[d]
$\Delta_{R1a}H°_0$	−4.3	(−)	−6.2	(−)	−4.1	(−)	−4.0	(−)	−2.2 ± 1.5
$\Delta_{R1d}H°_0$	−0.1	(−)	−9.6	(−)	−7.3	(−)	−7.1	(−)	−6.4 ± 1.0
$\Delta_{R2c}H°_0$	4.1	(−)	−3.4	(−)	−3.2	(−)	−3.1	(−)	−4.2 ± 1.1
$\Delta_{R1b}H°_0$	−31.2	−34.4	−38.5	−36.2	−36.3	−36.2	−36.2	−36.2	−36.2 ± 2.5
$\Delta_{R1c}H°_0$	−46.0	−49.3	−49.1	−50.3	−48.7	−50.3	−48.8	−50.3	−50.3 ± 2.5
$\Delta_{R1e}H°_0$	−19.9	−23.2	−25.3	−25.5	−25.2	−25.6	−25.2	−25.6	−25.6 ± 1.3
$\Delta_{R3a}H°_0$	−45.9	−42.9	−39.5	−43.9	−41.4	−43.9	−41.7	−43.9	−43.9 ± 2.1
$\Delta_{R3b}H°_0$	−31.1	−28.1	−28.9	−29.9	−29.0	−29.9	−29.1	−29.8	−29.8 ± 2.1
$\Delta_{R3i}H°_0$	−17.7	−16.6	−15.2	−18.0	−16.3	−18.1	−16.5	−18.0	−18.0 ± 3.1
$\Delta_{R3f}H°_0$	−28.4	−27.4	−22.8	−25.7	−25.0	−26.7	−25.3	−26.8	−26.8 ± 3.1
$\Delta_{R3g}H°_0$	−22.5	−21.5	−18.0	−20.8	−19.9	−21.7	−20.2	−21.6	−21.6 ± 3.1
$\Delta_{R3h}H°_0$	−27.8	−26.8	−23.0	−25.9	−24.5	−26.2	−24.7	−26.2	−26.2 ± 3.1
MAD[e]	3.3	1.2	2.6	0.3	1.3	0.0	1.2	0.0	
LD[f]	8.3	2.4	4.4	1.1	2.5	0.1	2.2	0.0	

[a] Calculated directly from the ZPE-corrected total energies of H, C_2H_3, C_2H_4, C_6H_5, C_6H_6, styrene, and radicals **1**−**3** and **6**−**9**. [b] Calculated from the experimental enthalpies of formation of H, C_2H_3, C_2H_4, C_6H_5, C_6H_6, styrene, and the isodesmic enthalpies of formation of radicals **1**−**3** and **6**−**9** evaluated at the specified level of theory. [c] Notations from schemes 2, 4, and 5 are used for different branches of reactions R1−R3. [d] The benchmark values are based on the experimental and isodesmic enthalpies of formation from Table 3. [e] Mean absolute deviation. [f] Largest deviation.

and with the theoretical estimate of Marshall[63] obtained at the CCSD(T) level of theory extrapolated to the complete basis set. For vinyl and phenyl, the enthalpies of formation were recently reevaluated by Ervin and DeTuri[64] from the gas-phase acidities of ethylene[65] and benzene.[66] For benzyl, we have adopted the value of Ellison et al.,[67] which has the smallest error limits and agrees with the most reliable experimental[68−71] and theoretical[72] determinations. Finally, the isodesmic enthalpy of formation of the C_6H_7 radical has been derived in our previous study[6] of the H + C_6H_6 reaction.

Combining our best estimates of the enthalpies of reactions R7−R13 with the enthalpies of formation of CH_4, C_2H_5, C_2H_6, C_3H_8, C_6H_5, C_6H_6, C_6H_7, styrene, and benzyl from Table 3, we obtain the isodesmic enthalpies of formation for radicals **1**−**3** and **6**−**9**, also listed in Table 3. The rather conservative error bars assigned to these enthalpies are sums of the theoretical and experimental uncertainties of all thermodynamic parameters used in the isodesmic reaction analysis. Our predicted standard enthalpy of formation of **2** is within the uncertainty limits of the most recent experimental value determined from the time-resolved photoacoustic calorimetry study.[71] Isodesmic enthalpies of formation of **1**−**3** also agree well with the earlier estimates of these quantities[58,73−75] obtained from the group-additive schemes and empirical correlations (see Table 3).

III.4. Accuracy of the Theoretical Energetic Parameters. Experimental and isodesmic enthalpies of formation of various species from Table 3 can be used to calculate the benchmark reaction enthalpies for different branches of reactions R1−R3 which can be compared to the values predicted by theoretical methods. In the following, the reaction enthalpy derived from the isodesmic analysis at a given level of theory, that is, using a combination of the isodesmic and experimental enthalpies of formation of the reactants and products, will be referred to as the *isodesmic enthalpy of reaction*, as opposed to the *direct enthalpy of reaction* which is calculated from the ZPE-corrected total energies of the reactants and products. In general, isodesmic enthalpies of reactions derived at different levels of theory are much less scattered and more reliable than the corresponding values calculated directly. The close agreement between the direct and isodesmic enthalpies calculated at a given level of theory is a good indicator of the accuracy of the theoretical predictions.

The performance of selected DFT and G2M methods is examined in Table 4. Energetic parameters calculated by other

methods, for example, (R/U)MP2, PMP4, (R/U)CCSD(T), are given in the Supporting Information (Tables S4−S8). As follows from Table 4, the B3LYP density functional performs rather poorly in the direct prediction of the energetics of reactions R1−R3, with errors often in excess of 5 kcal/mol and as much as 8.3 kcal/mol for reaction R2d. However, the isodesmic enthalpies of reactions calculated with this functional are substantially improved so that they are typically within the uncertainty limits of the benchmark values.

At the higher level, we have examined the differences in the energetics predicted by the G2M schemes, using spin-restricted versus spin-unrestricted formalisms. The direct enthalpies calculated by the G2M(UCC6) method deviate from the benchmark values by up to 4.4 kcal/mol. The errors can be tied to the unbalanced spin contamination of the UHF wave functions for open-shell reactants and products. Various branches of reaction R3 are affected the most, because the UHF wave function of the H-atom is a pure doublet ($<S^2> = 0.75$), whereas the radicals produced by reaction R3 are heavily spin-contaminated ($<S^2> = 1.3−1.5$). The replacement of the spin-unrestricted calculations with their spin-restricted analogues in the G2M(RCC6) scheme improves the calculated energetic parameters by 1−3 kcal/mol.

The G2M(RCC6) and G2M(RCC5) methods provide the most reliable energetic parameters. The direct enthalpies of reactions calculated by these methods differ by less than 0.5 kcal/mol, and they are typically within the uncertainty limits of the corresponding benchmark values (see Table 4). However, some deviations appear to be systematic. For instance, the C−H bond dissociation energy in radicals **6**−**9** is underestimated by 1.5 kcal/mol at the G2M(RCC5) level and by 1.7−1.8 kcal/mol at the G2M(RCC6) level. The error increases to 2.2−2.5 kcal/mol for the C−H bond dissociation energy in radical **2**. Thus, the performance of the G2M method deteriorates for radicals with a larger degree of π-electron delocalization, which probably require a larger basis set, as well as an explicit inclusion of the valence-core correlation, to fully recover electron correlation effects responsible for the unaccounted 1.5−2.5 kcal/mol in the stabilization energy of radicals **2** and **6**−**9** relative to H + styrene.

Homolytic bond dissociation energies for various types of the C−H bonds adjacent to radical centers have been analyzed by Zhang[76] with the aid of CBS-4 (complete basis set) model calculations. Zhang's $D_0°(\mathbf{1}) = 29.7$ kcal/mol and $D_0°(\mathbf{2}) = 44.6$

TABLE 5: Transition State Theory Rate Constants Calculated for Elementary Reactions[a]

reaction	log A[b]	n	E_a/kcal mol^{-1}	comment
$C_6H_5 + C_2H_4 \rightarrow C_6H_6 + C_2H_3$ (R1a)	−2.025	4.470	4.470	c,d
$C_6H_6 + C_2H_3 \rightarrow C_6H_5 + C_2H_4$ (R2a)	−0.389	4.020	8.802	c,d
$C_6H_5 + C_2H_4 \rightarrow$ **1** (R1b)	3.606	2.640	1.459	c,d
1 $\rightarrow C_6H_5 + C_2H_4$ (R-1b)	11.235	0.783	38.704	c,d
1 $\rightarrow C_6H_5C_2H_3 + H$ (R-3b)	6.262	2.081	33.207	c
1 $\rightarrow C_6H_5C_2H_3 + H$ (R-3b)	6.579	1.991	32.106	d
$C_6H_5C_2H_3 + H \rightarrow$ **1** (R3b)	5.895	2.248	3.795	c
$C_6H_5C_2H_3 + H \rightarrow$ **1** (R3b)	6.212	2.158	1.994	d
1 $\rightarrow$ **2** (500−2500 K)	5.775	2.074	29.582	c,d
(300−500 K)	−108.005	38.618	−5.222	c
(300−500 K)	−109.008	38.942	−5.517	d
2 $\rightarrow$ **1** (500−2500 K)	7.364	1.736	42.956	c
(300−500 K)	−107.852	38.728	7.626	c
2 $\rightarrow$ **1** (500−2500 K)	7.362	1.737	44.456	d
(300−500 K)	−108.855	39.051	8.831	d
2 $\rightarrow C_6H_5C_2H_3 + H$ (R-3a)	8.095	1.685	44.040	c
2 $\rightarrow C_6H_5C_2H_3 + H$ (R-3a)	8.573	1.550	44.609	d
$C_6H_5C_2H_3 + H \rightarrow$ **2** (R3a)	6.597	2.059	1.522	c
$C_6H_5C_2H_3 + H \rightarrow$ **2** (R3a)	7.075	1.925	−0.108	d
1 $\rightarrow$ **3** (500−2500 K)	5.109	2.017	25.225	c,d
(300−500 K)	−45.287	18.151	9.485	c,d
3 $\rightarrow$ **1** (500−2500 K)	5.151	2.052	14.421	c,d
(300−500 K)	−45.633	18.305	−1.476	c,d
1 $\rightarrow$ **4**	8.138	1.098	14.221	c,d
4 $\rightarrow$ **1**	12.591	0.253	3.694	c,d
1 $\rightarrow$ **5**	8.150	1.063	30.035	c,d
5 $\rightarrow$ **1**	11.936	0.474	11.755	c,d
6 $\rightarrow C_6H_5C_2H_3 + H$ (R-3i)	7.570	1.637	23.858	c
6 $\rightarrow C_6H_5C_2H_3 + H$ (R-3i)	7.872	1.551	23.435	d
$C_6H_5C_2H_3 + H \rightarrow$ **6** (R3i)	6.128	2.160	6.251	c
$C_6H_5C_2H_3 + H \rightarrow$ **6** (R3i)	6.430	2.074	4.428	d
7 $\rightarrow C_6H_5C_2H_3 + H$ (R-3f)	10.361	1.096	30.229	c
7 $\rightarrow C_6H_5C_2H_3 + H$ (R-3f)	10.672	1.008	29.925	d
$C_6H_5C_2H_3 + H \rightarrow$ **7** (R3f)	7.607	1.840	3.56	c
$C_6H_5C_2H_3 + H \rightarrow$ **7** (R3f)	7.918	1.752	1.756	d
8 $\rightarrow C_6H_5C_2H_3 + H$ (R-3 g)	9.198	1.339	26.054	c
8 $\rightarrow C_6H_5C_2H_3 + H$ (R-3 g)	9.477	1.260	25.624	d
$C_6H_5C_2H_3 + H \rightarrow$ **8** (R3 g)	7.185	1.972	4.810	c
$C_6H_5C_2H_3 + H \rightarrow$ **8** (R3 g)	7.464	1.893	2.979	d
9 $\rightarrow C_6H_5C_2H_3 + H$ (R-3h)	9.737	1.255	30.376	c
9 $\rightarrow C_6H_5C_2H_3 + H$ (R-3h)	10.106	1.150	30.002	d
$C_6H_5C_2H_3 + H \rightarrow$ **9** (R3h)	6.758	1.986	4.244	c
$C_6H_5C_2H_3 + H \rightarrow$ **9** (R3h)	7.127	1.882	2.471	d
6 $\rightarrow C_2H_3 + C_6H_6$ (R-2b)	13.247	0.234	28.334	c
6 $\rightarrow C_2H_3 + C_6H_6$ (R-2b)	13.251	0.233	28.837	d
$C_2H_3 + C_6H_6 \rightarrow$ **6** (R2b)	4.140	2.583	7.045	c
$C_2H_3 + C_6H_6 \rightarrow$ **6** (R2b)	4.144	2.581	5.048	d

[a] Fitted to the modified Arrhenius form: $k = AT^n \exp(-E_a/RT)$. $T = 250-2500$ K, unless noted otherwise. [b] The units of A are s^{-1} for unimolecular reactions and cm^3 mole^{-1} s^{-1} for bimolecular reactions. [c] Based on the G2M(RCC5) energetics from Figure 1. [d] Based on the adjusted energetic parameters (as described in sections III.5.B and III.5.C).

kcal/mol are in good agreement with our predictions of 29.8 ± 2.1 kcal/mol and 43.9 ± 2.1 kcal/mol, respectively.

The quality of the theoretical barriers of reactions is more difficult to assess, but common trends can be inferred for similar types of reactions from correlations between theoretical activation parameters and experimental kinetic data. As follows from the Appendix, the G2M(RCC5) barrier for the phenyl radical addition to acetylene is sufficiently accurate to account for the available experimental kinetic data. The theoretical barrier for the $C_6H_5 + C_2H_4$ addition reaction is expected to be of similar quality. On the other hand, the G2M(RCC5) barrier for H-addition to benzene is overestimated by ∼2 kcal/mol (see the Appendix) which correlates with the 1.4 kcal/mol error in the reaction enthalpy. From the computational standpoint, the H-addition reactions to benzene and styrene rings are very similar so that similar errors can be expected in the theoretical energies. Indeed, the G2M(RCC5) method underestimates the C−H bond dissociation energies in radicals **6−9** and C_6H_7 by virtually the same amount of 1.4−1.5 kcal/mol. By analogy with

the C_6H_6 + H reaction, the barriers for H-addition at different sites in styrene are likely to be ∼2 kcal/mol lower than the G2M(RCC5) values. For other reaction barriers, we tentatively assign a similar uncertainty of ±2 kcal/mol. With these provisions in mind we proceed to calculate the total and branching rate constants for reactions R1−R3.

III.5. Rate Constant Calculations. The rate constant calculations for reactions R1−R3 were performed with the ChemRate program,[42] assuming the mechanisms given in Schemes 2, 4, and 5. Molecular parameters used in the rate constant calculations are listed in the Supporting Information (Tables S1, S2). Initially, the G2M(RCC5) energetic parameters shown in Figure 1 were consistently employed. Then we examined the effect of the anticipated theoretical errors on the calculated kinetic data. As alluded to above, the errors in the G2M(RCC5) energies are expected to be within the limits of chemical accuracy (±2 kcal/mol). Table 5 summarizes the canonical TST rate constants with Eckart tunneling corrections calculated for all elementary reactions included in Schemes 2,

Quantum Chemical/RRKM-ME Computational Study

J. Phys. Chem. A, Vol. 108, No. 45, 2004 **9709**

4, and 5. The effective total and branching rate constants deduced from the RRKM/ME analysis will be presented separately for reactions R1−R3.

III.5.A. $C_6H_5 + C_2H_4$ Reaction. Parts A and B of Figure 4 illustrate effective total and branching rate constants for reaction R1 together with the available experimental data from Table 1 at different P and T. A strong curvature of the Arrhenius plot of k_{R1} is a sign of a changing mechanism in different regimes. At $T < 1400$ K, the major competition is between branches originating from the C_6H_5-addition to ethylene. Let us denote them as R1add. They lead either to the phenylation products (R1d) or to the stabilized radicals **1**, **2**, **3**, **5** (R1s = R1b + R1c + R1e + R1f). The H-abstraction channel (R1a) quickly gains in importance at $T > 1400$ K and becomes dominant at higher T. The corresponding rate constant can be expressed as $k_{R1a}(250-2500 \text{ K}) = (9.45 \times 10^{-3})T^{4.47} \exp(-(2250 \pm 1000)/T)$ cm^3 mol^{-1} s^{-1}, where an uncertainty of ± 2 kcal/mol has been assigned to the theoretical barrier.

The effective total rate constant of the C_6H_5-addition to ethylene, $k_{R1add} = k_{R1d} + k_{R1s}$, is essentially independent of P both in the low- and high-T regimes and can be expressed as $k_{R1add} = (4.41 \times 10^5)T^{1.96} \exp(-971/T)$ cm^3 mol^{-1} s^{-1}. Its effective nature is due to the fact that a fraction of the initially produced intermediates decomposes back to the reactants at high T, causing a deviation from the TST predictions. In general, the k_{R1add} effective rate constant is expected to exhibit P-dependence whenever there is a major competition between stabilization and decomposition back to the reactants. However, this condition is not realized at high T, where reactive intermediates are thermally unstable and the dominant pathways are either decomposition back to the $C_6H_5 + C_2H_4$ or H-elimination producing styrene (R1d) so that $k_{R1add} \sim k_{R1d}$, independent of P. Stabilization channels are important at low T. However, the decomposition via TS1 is energetically less favorable than the H-elimination pathways via TS6(α,β) grouped into channel R1d. As a result, at low T the major channels are either stabilization (R1s = R1b + R1c + R1e + R1f) or phenylation (R1d), so that $k_{R1add} = k_{R1s} + k_{R1d} \sim k_{R1add}^{TST}$, independent of P. The corresponding low-T branching rate constants, k_{R1s} and k_{R1d}, approach the TST limit, k_{R1add}^{TST}, at high and low P, respectively.

The present analysis also provides additional insights into the role of various pathways and intermediates in the mechanism of reaction R1. Figure 5 gives the time-dependent composition of the C_8H_9 radicals produced by this reaction. Initially, reaction R1 yields isomer **1**, which then equilibrates with the more stable isomer **2**. Wells **1** and **2** effectively trap the reactive intermediates at low T, and in general, their secondary bimolecular reactions should be included in the kinetic modeling along with reaction R1. However, the latter are specific to the experimental system, so in the present analysis we only consider unimolecular transformations of **1** and **2**. At low T and high P, **1** is the major product of reaction R1, because collisional stabilization of the chemically activated **1**† occurs faster than isomerization or decomposition. At higher T, well **2** quickly becomes the most populated. At the same time, the H-elimination pathways gain in importance (see Figure 4B). Typically, a major fraction of the phenylation products (R1d) is formed directly from **1**. However, the reaction flux through TS6(β) is significant at high T, and at a given P the fraction of the H + styrene formed via TS6(β) reaches its maximum at a certain T_P. For example, up to 60% of H + styrene is formed via TS6(β) at $P = 0.1$ Torr, $T_{P=0.1 \text{ Torr}} = 800$ K, and up to 45% at $P = 1$ atm, $T_{P=1 \text{ atm}} = 1400$ K.
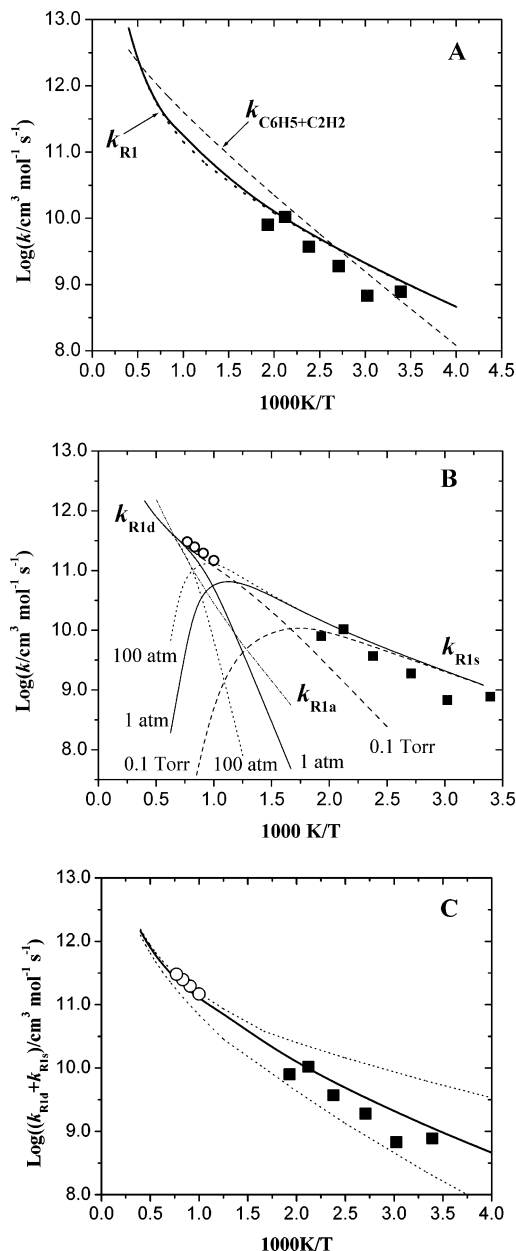
Figure 4. Experimental and calculated total and branching rate constants for reaction R1. Plot A: solid curve, k_{R1}(100 atm); dotted curve, k_{R1}(0.1 Torr); dashed curve, $k_{C6H5+C2H2}$. Plot B: solid curves, k_{R1d}(1 atm) and k_{R1s}(1 atm); dashed curves, k_{R1d}(0.1 Torr) and k_{R1s}(0.1 Torr); dotted curves, k_{R1d}(100 atm) and k_{R1s}(100 atm); dash-dotted curve, k_{R1a}. Plot C: solid curve, k_{R1add}; dotted curves illustrate the sensitivity of k_{R1add} to the variation of the C_6H_5-addition barrier by ± 1 kcal/mol. Experimental data is taken from ref 12 (k_{R1d}, $\bigcirc$) and ref 14 (k_{R1}, $\blacksquare$). Calculated rate constants (in cm^3 mol^{-1} s^{-1}): k_{R1a}(250−2500 K) = $(9.45 \times 10^{-3})T^{4.47} \exp(-2250/T)$; k_{R1add}(250−2500 K) = ($k_{R1d} + k_{R1s}$) = $(4.41 \times 10^5)T^{1.96} \exp(-971/T)$; k_{R1b}(0.1 Torr, 250−600 K) = $(5.49 \times 10^{32})T^{-7.38} \exp(-3690/T)$; k_{R1b}(1 atm, 250−800 K) = $(7.06 \times 10^5)T^{1.89} \exp(-993/T)$; k_{R1b}(100 atm, 250−1000 K) = $(4.95 \times 10^4)T^{2.28} \exp(-866/T)$; k_{R1c}(0.1 Torr, 250−800 K) = $(4.29 \times 10^{44})T^{-10.62} \exp(-7290/T)$; k_{R1c}(1 atm, 300−1000 K) = $(2.34 \times 10^{-26})T^{12.23} \exp(-514/T)$; k_{R1c}(100 atm, 400−1200 K) = $(1.57 \times 10^{-31})T^{13.7} \exp(-1380/T)$; k_{R1d}(0.1 Torr, 400−2500 K) = $(3.83 \times 10^{13})T^{-0.23} \exp(-4146/T)$; k_{R1d}(1 atm, 800−2500 K) = $(3.62 \times 10^{28})T^{-4.24} \exp(-12010/T)$; k_{R1d}(100 atm, 1000−2500 K) = $(1.50 \times 10^{45})T^{-8.65} \exp(-21350/T)$.

The experimental points[12,14] shown in Figure 4B are in good agreement with the calculated rate constants (within a factor of 2 or better) without any adjustment of the G2M(RCC5) energetic parameters. In Figure 4C we have illustrated the sensitivity of
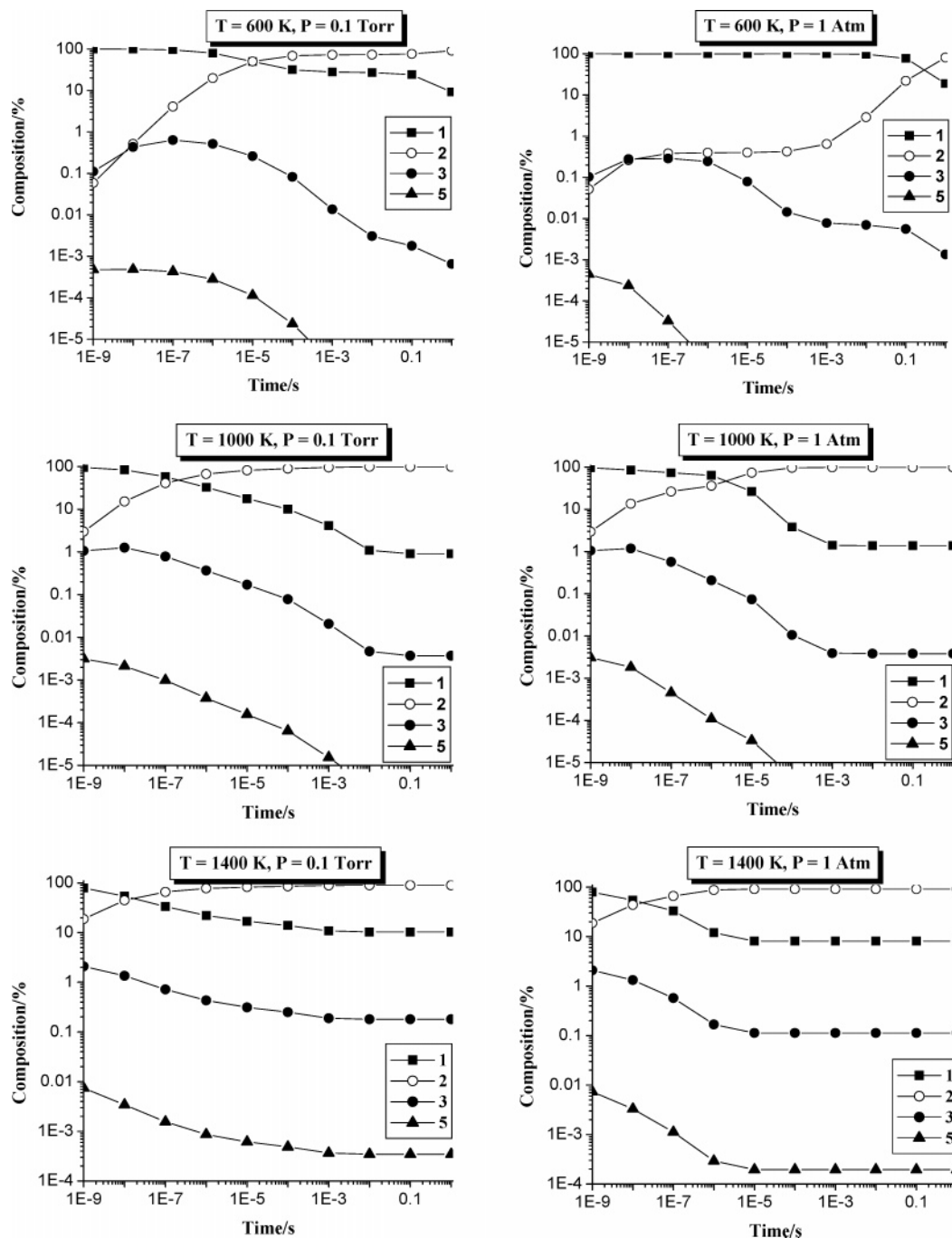
Figure 5. Time-dependent composition of the intermediates produced by the $C_6H_5 + C_2H_4$ reaction at selected P and T.

the calculated k_{R1add} rate constant to the variation of the addition barrier (TS1) by ± 1 kcal/mol. A comparison with the low-T experimental data of Yu and Lin[14] suggests that the accuracy of the G2M(RCC5) barrier is better than 1 kcal/mol. The k_{R1d} rate constant measured by Stein et al.[12] is also sensitive to the H-elimination barriers (TS6(α,β)). As discussed in the previous section, the H-addition barriers to styrene may be overestimated by $\sim$2 kcal/mol at the G2M(RCC5) level. Lowering TS6(α) and TS6(β) by 2 kcal/mol increases the calculated k_{R1d} rate constant by up to 25% in the experimental T range of Stein et al., which brings it even closer (within 10%) to the experimental values.

An interesting comparison can be made between the total rate constants of the C_6H_5 radical reactions with C_2H_4 (k_{R1}) and C_2H_2 ($k_{C6H5+C2H2}$). The latter is available from our previous investigation[8] (see also the Appendix). As shown in Figure 4A,

the k_{R1} rate constant is faster at low T, because the barrier of the C_6H_5 addition to a double C−C bond is lower than to a triple C−C bond. However, the entropy of activation is less negative for the phenyl addition to C_2H_2. This factor is responsible for a higher $k_{C6H5+C2H2}$ rate constant in the middle- to high-T ranges. At very high T, the k_{R1} rate constant again becomes faster than $k_{C6H5+C2H2}$, because of the contribution from the H-abstraction, which is only important for reaction R1.

III.5.B. $C_2H_3 + C_6H_6$ Reaction. The total and branching rate constants for reaction R2 calculated on the basis of the G2M(RCC5) energetics are shown in parts A and B of Figure 6. Mechanistically, this reaction is similar to reaction R1 and somewhat simpler, because only one C_8H_9 isomer is formed by the C_2H_3-addition to benzene. The H-abstraction channel is predicted to be dominant at high T, with $k_{R2a}^{TST} =$

Quantum Chemical/RRKM-ME Computational Study

J. Phys. Chem. A, Vol. 108, No. 45, 2004 **9711**

$0.408T^{4.02}\exp(-(4430\pm1000)/T)$ cm^3 mol^{-1} s^{-1}. At lower T, the main reaction mode is the C_2H_3-addition to benzene, followed by deactivation of radical **6** (R2b) competing with its decomposition to H + $C_6H_5C_2H_3$ (R2c) and back to the C_2H_3 + C_6H_6. In the middle-T range (500–1000 K), the total effective rate constant k_{R2} exhibits a moderate P-dependence: $k_{R2} \sim k_{R2b}$ $\rightarrow k_{R2}^{TST}$ at high P, whereas at low P (in the absence of stabilizing collisions), $k_{R2} \ll k_{R2}^{TST}$, because a major fraction of the initially formed **6**† decomposes back to the reactants. The latter pathway is favored over the H-elimination at $T > 500$ K because of the considerably higher entropy of TS9 compared to TS6(ipso), which is mainly due to a less hindered internal rotation of the vinyl group in TS9.

As follows from Figure 6B, the calculated k_{R2c} rate constant of the H-for-C_2H_3 substitution in benzene significantly (by a factor of 5) underestimates the experimental values of Stein et al.[12] Although the latter values have been measured indirectly and have a relatively large uncertainty of a factor of 2.6, the deviation of the calculated rate constants is too large. We believe the G2M energetics is at fault. In an effort to systematically correct the G2M(RCC5) energetic parameters, we have used more reliable experimental and isodesmic enthalpies of reactions (best values from Table 4): $\Delta_{R2c}H^\circ_0 = -4.2$ kcal/mol; $\Delta_{R3i}H^\circ_0 = -18.0$ kcal/mol. In addition, the G2M(RCC5) barriers for the C_2H_3-addition to benzene (TS9) and H + styrene ipso-addition (TS6(ipso)) have been systematically lowered by 2 kcal/mol. Such an adjustment is in line with the previously found errors[6,7] in the G2M barriers for H, CH$_3$, and OH radical additions to benzene (see also the Appendix). The corrected 0 K barriers amount to 6.1 kcal/mol (TS9) and 7.3 kcal/mol (TS6(ipso)). As shown in Figure 6C, the k_{R2c} rate constant calculated from the adjusted energetic parameters is in excellent agreement with the experimental values of Stein et al.[12] The P,T-dependence of the modified k_{R2b} and k_{R2c} rate constants is qualitatively similar to that exhibited by the G2M-based rate constants. However, the P-dependence of the total rate constant becomes less pronounced, so it can be effectively represented as $k_{R2add}(250-2500 \text{ K}) = (k_{R2b} + k_{R2c}) = (1.87 \times 10^7)T^{1.47}\exp(-2785/T)$ cm^3 mol^{-1} s^{-1}, independent of P.

III.5.C. H + $C_6H_5C_2H_3$ Reaction. In the present work, only H-addition channels of reaction R3 have been investigated. By analogy to reactions R1 and R2, the H-abstraction channels are expected to be important for the mechanism of reaction R3 only at relatively high T.

Even without the H-abstraction channels, the mechanism of reaction R3 depicted in Scheme 5 appears much more complex than those of reactions R1 and R2. However, most of the branches of reaction R3 are not coupled with each other, which greatly simplifies the theoretical analysis. The calculated total and branching rate constants for reaction R3 are shown in Figure 7. We present the results for a single $P = 1$ atm, because they are sufficient to describe the general trends and no experimental data is available for specific comparisons.

In the low- and middle-T ranges (up to 1200 K), the H-addition to styrene preferably occurs at the β-position (R3a), producing radical **2** with high regioselectivity. The second most important channel is the ortho-addition (R3f). The branching rate constants for α-, meta- and para-additions are of similar magnitude, which is more than one order smaller than that of the k_{R3a} rate constant. The fraction of radicals **3**, **5**, and **6** in the pool of the C$_8$H$_9$ isomers produced by reaction R3 is negligibly small.

Provided the T is high enough ($T > 1200$ K), the reactive intermediates are not stabilized despite numerous collisions with
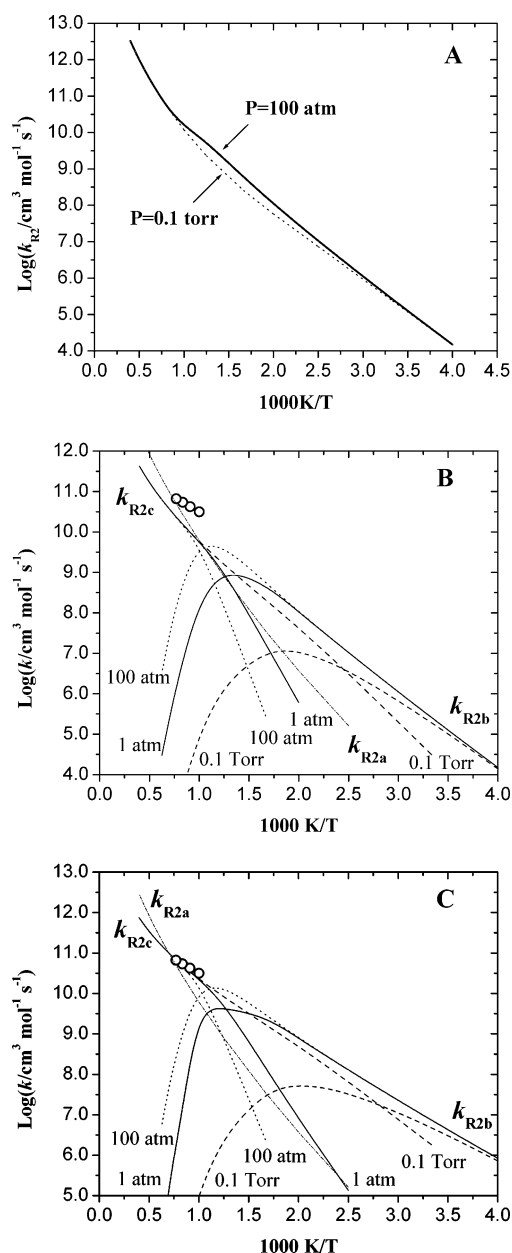
Figure 6. Total and branching rate constants for reaction R2 calculated using the G2M(RCC5) energetics from Figure 1 (Plots A and B) and adjusted energetic parameters (Plot C). Plot A: solid curve, $k_{R2}(100$ atm); dotted curve, $k_{R2}(0.1$ Torr). Plot B: solid curves, $k_{R2b}(1$ atm) and $k_{R2c}(1$ atm); dashed curves, $k_{R2b}(0.1$ Torr) and $k_{R2c}(0.1$ Torr); dotted curves, $k_{R2b}(100$ atm) and $k_{R2c}(100$ atm); dash-dotted curve, k_{R2a}. Plot C: notations are the same as in Plot B, but the rate constants are calculated from the adjusted energetic parameters (see text). Experimental data is taken from ref 12 (k_{R2c}, $\bigcirc$). Calculated rate constants from Plot C (in cm^3 mol^{-1} s^{-1}): $k_{R2a}(250-2500$ K) = $0.408T^{4.02}\exp(-(4430\pm1000)/T)$; $k_{R2add}(250-2500$ K) = $(k_{R2b} + k_{R2c})$ = $(1.87 \times 10^7)T^{1.47}\exp(-2785/T)$; $k_{R2b}(0.1$ Torr, 250–600 K) = $(4.38 \times 10^{44})T^{-11.7}\exp(-6166/T)$; $k_{R2b}(1$ atm, 250–800 K) = $(4.28 \times 10^{20})T^{-2.92}\exp(-4470/T)$; $k_{R2b}(100$ atm, 250–1000 K) = $(9.05 \times 10^{15})T^{-1.31}\exp(-4007/T)$; $k_{R2c}(0.1$ Torr, 300–2500 K) = $(1.45 \times 10^8)T^{1.24}\exp(-3362/T)$; $k_{R2c}(1$ atm, 600–2500 K) = $(1.08 \times 10^{18})T^{-1.44}\exp(-7930/T)$; $k_{R2c}(100$ atm, 800–2500 K) = $(1.24 \times 10^{26})T^{-3.59}\exp(-12240/T)$.

bath gas, because a large fraction of these collisions are activating. This T marks the threshold of thermal stability of radical **2**, above which it either decomposes back to the H + $C_6H_5C_2H_3$ or breaks down to C_6H_5 + C_2H_4 (R3d) bypassing radical **1**†. Although the ipso-addition via TS6(i) accounts for a tiny fraction of the total rate at low T, it becomes the second
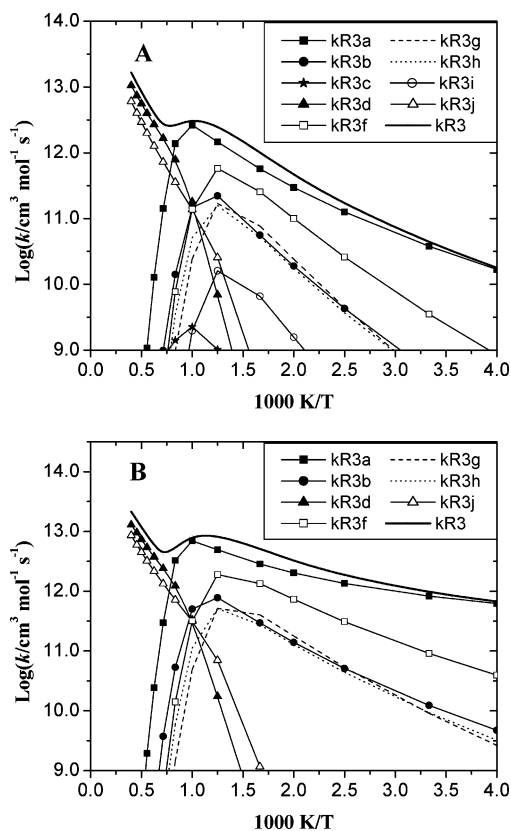
Figure 7. Total and branching rate constants for reaction R3 at $P = 1$ atm calculated either using the G2M(RCC5) energetics from Figure 1 (Plot A) or from the adjusted energetic parameters (Plot B). Calculated rate constants from Plot B (in $cm^3 \ mol^{-1} \ s^{-1}$): $k_{R3a}(250-1000 \ K) = (1.25 \times 10^7)T^{1.91} \exp(65/T)$; $k_{R3b}(250-800 \ K) = (4.20 \times 10^5)T^{2.33} \exp(-890/T)$; $k_{R3d}(500-2500 \ K) = (1.63 \times 10^{37})T^{-6.31} \exp(-15940/T)$; $k_{R3f}(250-800 \ K) = (3.11 \times 10^{13})T^{-0.12} \exp(-1520/T)$; $k_{R3 \ g}(250-800 \ K) = (4.73 \times 10^{17})T^{-1.53} \exp(-2670/T)$; $k_{R3h}(250-800 \ K) = (1.31 \times 10^{11})T^{0.53} \exp(-1675/T)$; $k_{R3j}(600-2500 \ K) = (5.62 \times 10^{24})T^{-3.0} \exp(-9980/T)$.

most important channel at high T, when radical **6**† decomposes to $C_2H_3 + C_6H_6$ (R3j).

As alluded to above, we anticipate that the G2M(RCC5) method may overestimate the barriers of H-addition to styrene by ~2 kcal/mol and underestimate the C—H bond dissociation energies in **1**, **2**, **6**, **7**, **8**, **9** (see Table 4). Therefore, we have recalculated the rate constants for reaction R3, using the following adjusted energetic parameters: $\Delta_{R3a}H°_0 = -43.9$ kcal/mol; $\Delta_{R3b}H°_0 = -29.8$ kcal/mol, $\Delta_{R3d}H°_0 = 6.4$ kcal/mol, $\Delta_{R3f}H°_0 = -26.8$ kcal/mol, $\Delta_{R3 \ g}H°_0 = -21.6$ kcal/mol, $\Delta_{R3h}H°_0 = -26.2$ kcal/mol, $\Delta_{R3i}H°_0 = -18.0$ kcal/mol, $\Delta_{R3j}H°_0 = 4.2$ kcal/mol, and the barriers for H-addition to styrene (TS6) and C_2H_3-addition to benzene (TS9) lowered by 2 kcal/mol. As follows from a comparison of the rate constants shown in parts A and B of Figure 7, replacing the G2M(RCC5) energetic parameters with the adjusted values enhances the low-T rate constants but does not change significantly the qualitative description of the mechanism of reaction R3. Unfortunately, no experimental kinetic data is available to shed further light on the mechanism of reaction R3 and to test the accuracy of our predicted rate constants.

IV. Conclusions

The mechanisms of reactions R1—R3 are investigated quantum chemically by the G2M method. A high-level RCCmax (IRCMax(RCCSD(T)//B3LYP)) optimization procedure is em-

ployed as an affordable way of refining the TS geometries for radical addition reactions, where the standard B3LYP method overestimates the lengths of the forming bonds. Reliable thermochemistry of individual species on the [C_8H_9] PES is established through isodesmic reaction analysis. Judging from the comparisons with available benchmark values, the accuracy of the G2M energetic parameters improves upon replacement of the spin-unrestricted calculations with their spin-restricted analogues. However, even at the highest level of theory (G2M(RCC5)) small systematic errors (1—2 kcal/mol) are identified in the enthalpies and barriers for radical additions producing π-radicals with a large degree of electron delocalization.

The present study provides a consistent set of kinetic parameters for the $C_6H_5 + C_2H_4$, $C_2H_3 + C_6H_6$, and H + $C_6H_5C_2H_3$ reactions derived from the comprehensive RRKM-ME analysis. The kinetic models (Schemes 2, 4, 5) including all important product branches are constructed for reactions R1—R3 on the basis of the quantum chemical calculations. Under combustion conditions ($T > 1000$ K), all three sets of reactants are closely interconnected by the reversible H-abstraction (R1a/R2a), phenylation (R1d), vinylation (R2c), and desubstitution (R3d, R3j) reactions. In addition, relatively long-lived radicals **1**, **2**, and **7** are produced by reactions R1—R3 with high efficiency. The secondary bimolecular reactions of these radicals may also be important, especially for PAH formation mechanisms. The rate constants calculated in this work using systematically adjusted theoretical energetic parameters agree with available experimental kinetic data for reactions R1 and R2 well within the experimental scatter. Such degree of consistency raises our confidence in the accuracy of the employed energetics and calculated rate constants, which can be used in the modeling of HC combustion and pyrolysis.

In a final note, the PES for reactions R1—R3 investigated in this study lays the groundwork for detailed studies of the mechanism and product distribution for other reactions on the [C_8H_9] molecular PES, such as fulvene + C_2H_3, benzyne + C_2H_5, H + C_8H_8 (various isomers), and so forth.

Appendix. Rate Constants for the $C_6H_5 + C_2H_2$ and C_6H_6 + H Addition Reactions

In this section, we briefly revisit the $C_6H_5 + C_2H_2$ and C_6H_6 + H addition reactions, which were the subjects of our recent computational studies.[6,8] Both reactions are exothermic and have relatively loose TSs. In our previous investigations, we reported the PES for these reactions calculated by several G2M models, employing the molecular structures optimized by the B3LYP/6-311++G(d,p) method. In this work, we have utilized the more accurate RCCmax procedure to locate loose TSs on the reaction paths optimized by the B3LYP method. The molecular parameters of the reoptimized TSs are collected in the Supporting Information.

The refined TS structures are tighter than those obtained from the standard B3LYP optimization: the lengths of the breaking C—C bond in TS($C_6H_5 + C_2H_2$) and the C—H bond in TS(C_6H_6

Quantum Chemical/RRKM-ME Computational Study

J. Phys. Chem. A, Vol. 108, No. 45, 2004 **9713**
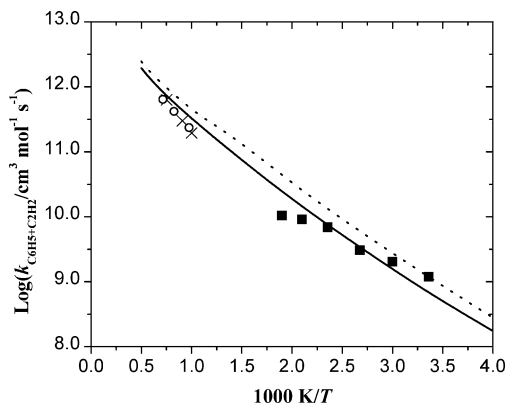
Figure A1. Experimental and calculated total rate constants for the $C_6H_5 + C_2H_2$ reaction. Theoretical curves: solid line, $k_{C6H5+C2H2} = (1.26 \cdot 10^9)T^{1.10} \exp(-2060/T)$ cm^3 mol^{-1} s^{-1}, calculated using the TS structure located on the B3LYP reaction path by the RCCmax procedure, with a G2M(RCC5) barrier of 3.75 kcal/mol; dotted line, $k_{C6H5+C2H2}$ calculated using the TS optimized by the B3LYP/6-311++G(d,p) method, with a G2M(RCC5) barrier of 3.70 kcal/mol. Experimental data: (○) Heckmann et al.;[15] (×) Stein et al.;[12] (■) Yu et al.[77]
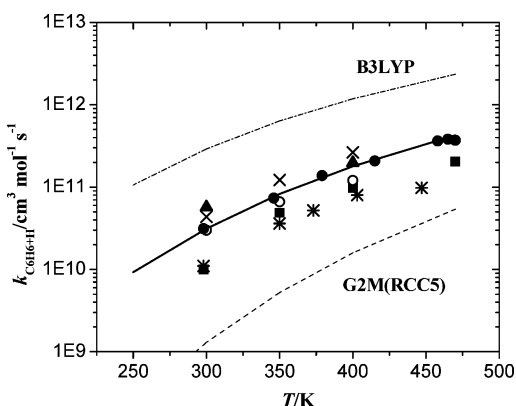
Figure A2. Experimental and calculated total rate constants of H-addition to benzene: solid line, $k_{C6H6+H} = (3.0 \times 10^{13}) \exp(-2040/T)$ cm^3 mol^{-1} s^{-1}, calculated using the TS structure optimized by the RCCmax method, with an adjusted barrier of 5.2 kcal/mol; dashed line, k_{C6H6+H} calculated using the G2M(RCC5)//RCCmax barrier of 7.2 kcal/mol; dash-dotted line, k_{C6H6+H} calculated from the B3LYP molecular and energetic parameters, with a barrier of 3.7 kcal/mol; (●) Nicovich, Ravishankara;[78] (*) Hoyermann et al.;[79] (■) Yang;[80] (▲) Kim et al.;[81] (×) Sauer, Mani;[82a] (○) Sauer, Ward.[82b]

+ H) change from 2.35 to 2.28 Å and from 1.87 to 1.77 Å, respectively. The barrier for H-addition to benzene predicted by the G2M(RCC5) method becomes 7.2 kcal/mol, versus 6.6 kcal/mol before reoptimization. The G2M(RCC5) barrier for C_6H_5-addition to acetylene becomes 3.75 kcal/mol, just 0.05 kcal/mol higher than our old value.

Previously, theoretical energetic parameters required adjustments in order to account for the available experimental kinetic data. In particular, a fitted barrier of 4.1 kcal/mol was recommended for the $C_6H_5 + C_2H_2$ reaction.[8] The $k_{C6H5+C2H2}$ rate constant calculated in this work from the reoptimized molecular and energetic parameters shows good agreement with experimental values[12,15,77] without any empirical corrections (see Figure A1).

For the $C_6H_6 + H$ addition reaction, the accurate reaction enthalpy of -21.3 ± 2.0 kcal/mol (at 0 K) was derived from the isodesmic reaction analysis; and the 0 K barrier of 5.2 kcal/mol allowed us to account for the most reliable experimental data.[78–82] Our previous best direct estimates of the reaction barrier (8.5 kcal/mol) and enthalpy (−18.7 kcal/mol) calculated

at the G2M(UCC5) level were systematically too high. The present G2M(RCC5) predictions, 7.2 kcal/mol for the barrier and −19.9 kcal/mol for the enthalpy, are closer to the accurate values, but still appear to be overestimated by 1−2 kcal/mol. In Figure A2, we illustrate the k_{C6H6+H} rate constant calculated using the G2M(RCC5) and B3LYP theoretical barriers and including the unsymmetric Eckart tunneling correction. The theoretical curves may be considered as the lower (G2M(RCC5)) and upper (B3LYP) bounds of k_{C6H6+H}. Apparently, the calculated rate constant is not very sensitive to the molecular structure of the TS, so the same fitted barrier of 5.2 kcal/mol applies to the TSs optimized by either a standard B3LYP method or a RCCmax procedure.

Supporting Information Available: Tables S1 and S2 contain the molecular parameters for all species and transition states calculated in this study. Tables S3−S8 contain detailed energetics of all stationary points calculated at various theoretical levels. This material is available free of charge via the Internet at http://pubs.acs.org.

References and Notes

(1) Frenklach, M. *Phys. Chem. Chem. Phys*. **2002**, *4*, 2028−2037.

(2) Richter, H.; Howard, J. B. *Prog. Energy Combust. Sci*. **2000**, *26*, 565−608.

(3) Richter, H.; Howard, J. B. *Phys. Chem. Chem. Phys*. **2002**, *4*, 2038−2055.

(4) Mebel, A. M.; Lin, M. C.; Yu, T.; Morokuma, K. *J. Phys. Chem. A* **1997**, *101*, 3189.

(5) Tokmakov, I. V.; Park, J.; Gheyas, S.; Lin, M. C. *J. Phys. Chem. A* **1999**, *103*, 3636.

(6) Tokmakov, I. V.; Lin, M. C. *Int. J. Chem. Kinet*. **2001**, *33*, 633−653.

(7) Tokmakov, I. V.; Lin, M. C. *J. Phys. Chem. A* **2002**, *106*, 11309−11326.

(8) Tokmakov, I. V.; Lin, M. C. *J. Am. Chem. Soc*. **2003**, *125*, 11397−11408.

(9) (a) Brouwer, L.; Muller-Markgraf, W.; Troe, J. *Ber. Bunsen-Ges. Phys. Chem* **1983**, *87*, 1031−1036. (b) Muller-Markgraf, W.; Troe, J. *J. Phys. Chem*. **1988**, *92*, 4914−4922. (c) Litzinger, T. A.; Brezinsky, K.; Glassman, I. *Combust. Flame* **1986**, *63*, 251. (d) Baldwin, R. R.; Lodhi, Z. H.; Scothard, N.; Walker, R. W. *Proc. Combust. Inst*. **1990**, *23*, 123−130. (e) Ellis, C.; Scott, M. S.; Walker, R. W. *Combust. Flame* **2003**, *132*, 291−304.

(10) (a) Ortiz de Montellano, P. R.; Watanabe, M. D. *Mol. Pharmacol*. **1987**, *31*, 213-219. (b) Leite, L. C. C.; Augusto, O. *Arch. Biochem. Biophys*. **1989**, *270*, 560. (c) Yamamoto, K.; Kawanishi, Sh. *Chem. Res. Toxicol*. **1992**, *5*, 440. (d) Justo, G. Z.; Livotto, P. R.; Duran, N. *Free Radical Biol. Med*. **1995**, *19*, 431−440.

(11) (a) Bevington, J. C.; Cywar, D. A.; Huckerby, T. N.; Senogles, E.; Tirrell, D. A. *Eur. Polym. J*. **1990**, *26*, 871−875. (b) Jenkins, A. D. *Polymer* **1999**, *40*, 7045−7058. (c) Skene, W. G.; Scaiano, J. C.; Yap, G. P. A. *Macromolecules* **2000**, *33*, 3536−3542.

(12) (a) Fahr, A.; Mallard, W. G.; Stein, S. E. *Proc. Combust. Inst.* **1986**, *21*, 825−831. (b) Fahr, A.; Stein, S. E. *Proc. Combust. Inst*. **1988**, *22*, 1023−1029.

(13) Preidel, M.; Zellner, R. *Ber. Bunsen-Ges. Phys. Chem*. **1989**, *93*, 1417.

(14) Yu, T.; Lin, M. C. *Combust. Flame* **1995**, *100*, 169−176.

(15) Heckmann, E.; Hippler, H.; Troe, J. *Proc. Combust. Inst*. **1996**, *26*, 543−550.

(16) Park, J.; Lin, M. C. *J. Phys. Chem. A* **1997**, *101*, 14−18.

(17) Colket, M. B., III; Seery, D. J.; Palmer, H. B. *Combust. Flame* **1989**, *75*, 343−366.

(18) Benson, S. W. *Int. J. Chem. Kinet*. **1989**, *21*, 233.

(19) Tsang, W.; Hampson, R. F. *J. Phys. Chem. Ref. Data* **1986**, *15*, 1087.

(20) (a) Fahr, A.; Laufer, A. H. *J. Phys. Chem*. **1990**, *94*, 726-9. (b) Fahr, A.; Laufer, A. H.; Klein, R.; Braun, W. *J. Phys. Chem*. **1991**, *95*, 3218−3224.

(21) Wallington, T. J.; Egsgaard, H.; Nielsen, O. J.; Platz, J.; Sehested, J.; Stein, T. *Chem. Phys. Lett*. **1998**, *290*, 363.

(22) Tonokura, K.; Norikane, Y.; Koshi, M.; Nakano, Y.; Nakamichi, S.; Goto, M.; Hashimoto, S.; Kawasaki, M.; Sulbaeck Andersen, M. P.; Hurley, M. D.; Wallington, T. J. *J. Phys. Chem. A* **2002**, *106*, 5908−5917.

(23) Gilbert, R. G.; Smith, S. C. *Theory of Unimolecular and Recombination Reactions*; Blackwell Scientific Publications: Oxford, 1990.

(24) Forst, W. *Theory of Unimolecular Reactions*; Academic Press: New York, 1973.

(25) Robinson, P. J.; Holbrook, K. A. *Unimolecular Reactions*; Wiley: New York, 1972.

(26) Frisch, M. J.; Trucks, G. W.; Schlegel, H. B.; Scuseria, G. E.; Robb, M. A.; Cheeseman, J. R.; Montgomery, J. A., Jr.; Vreven, T.; Kudin, K. N.; Burant, J. C.; Millam, J. M.; Iyengar, S. S.; Tomasi, J.; Barone, V.; Mennucci, B.; Cossi, M.; Scalmani, G.; Rega, N.; Petersson, G. A.; Nakatsuji, H.; Hada, M.; Ehara, M.; Toyota, K.; Fukuda, R.; Hasegawa, J.; Ishida, M.; Nakajima, T.; Honda, Y.; Kitao, O.; Nakai, H.; Klene, M.; Li, X.; Knox, J. E.; Hratchian, H. P.; Cross, J. B.; Adamo, C.; Jaramillo, J.; Gomperts, R.; Stratmann, R. E.; Yazyev, O.; Austin, A. J.; Cammi, R.; Pomelli, C.; Ochterski, J.; Ayala, P. Y.; Morokuma, K.; Voth, G. A.; Salvador, P.; Dannenberg, J. J.; Zakrzewski, V. G.; Dapprich, S.; Daniels, A. D.; Strain, M. C.; Farkas, O.; Malick, D. K.; Rabuck, A. D.; Raghavachari, K.; Foresman, J. B.; Ortiz, J. V.; Cui, Q.; Baboul, A. G.; Clifford, S.; Cioslowski, J.; Stefanov, B. B.; Liu, G.; Liashenko, A.; Piskorz, P.; Komaromi, I.; Martin, R. L.; Fox, D. J.; Keith, T.; Al-Laham, M. A.; Peng, C. Y.; Nanayakkara, A.; Challacombe, M.; Gill, P. M. W.; Johnson, B.; Chen, W.; Wong, M. W.; Gonzalez, C.; Pople, J. A. *Gaussian 03*, revision B.01; Gaussian, Inc.: Pittsburgh, PA, 2003.

(27) Amos, R. D.; Bernhardsson, A.; Berning, A.; Celani, P.; Cooper, D. L.; Deegan, M. J. O.; Dobbyn, A. J.; Eckert, F.; Hampel, C.; Hetzer, G.; Knowles, P. J.; Korona, T.; Lindh, R.; Lloyd, A. W.; McNicholas, S. J.; Manby, F. R.; Meyer, W.; Mura, M. E.; Nicklass, A.; Palmieri, P.; Pitzer, R.; Rauhut, G.; Schütz, M.; Schumann, U.; Stoll, H.; Stone, A. J.; Tarroni, R.; Thorsteinsson, T.; Werner, H.-J. *MOLPRO*, version 2002.6; University of Birmingham: Birmingham, UK, 2003.

(28) Mebel, A. M.; Morokuma, K.; Lin, M. C. *J. Chem. Phys.* **1995**, *103*, 7414.

(29) (a) Becke, A. D. *J. Chem. Phys.* **1993**, *98*, 5648. (b) Becke, A. D. *Phys. Rev. A* **1988**, *38*, 3098. (c) Lee, C.; Yang, W.; Parr, R. G. *Phys. Rev. B* **1988**, *37*, 785. (d) Stephens, P. J.; Devlin, F. J.; Chabalowski, C. F.; Frisch, M. J. *J. Phys. Chem.* **1994**, *98*, 11623.

(30) Pople, J. A.; Head-Gordon, M.; Raghavachari, K. *J. Chem. Phys.* **1987**, *87*, 5968.

(31) (a) Johnson, B. G.; Frisch, M. J. *Chem. Phys. Lett.* **1993**, *216*, 133. (b) Johnson, B. G.; Frisch, M. J. *J. Chem. Phys.* **1994**, *100*, 7429.

(32) The performance of the B3LYP functional for geometry optimization was assessed, for example, by the authors of the G2M (ref 28), G3//B3LYP (Baboul, A. G.; Curtiss, L. A.; Redfern, P. C.; Raghavachari, K. *J. Chem. Phys.* **1999**, *110*, 7650), and G3X (Curtiss, L. A.; Redfern, P. C.; Raghavachari, K.; Pople, J. A. *J. Chem. Phys.* **2001**, *114*, 108) model chemistries.

(33) *Computational Chemistry Comparison and Benchmark Database*; NIST Standard Reference Database Number 101; Johnson, R. D., III, Ed.; National Institute of Standards and Technology: Gaithersburg, MD, May 2003 (http://srdata.nist.gov/cccbdb/).

(34) Scott, A. P.; Radom, L. *J. Phys. Chem.* **1996**, *100*, 16502.

(35) (a) Koch, W.; Holthausen, M. C. *A Chemist's Guide to Density Functional Theory*, 2nd ed.; Wiley-VCH: New York, 2001. (b) Heuts, J. P. A.; Hilbert, R. G.; Radom, L. *J. Phys. Chem.* **1996**, *100*, 18997.

(36) (a) Gonzalez, C.; Schlegel, H. B. *J. Chem. Phys.* **1989**, *90*, 2154–2161. (b) Gonzalez, C.; Schlegel, H. B. *J. Phys. Chem.* **1990**, *94*, 5523–5527.

(37) Malick, D. K.; Petersson, G. A.; Montgomery, J. A., Jr. *J. Chem. Phys.* **1998**, *108*, 5704 and references therein.

(38) Saeys, M.; Reyniers, M.-F.; Marin, G. B.; Van Speybroeck, V.; Waroquier, M. *J. Phys. Chem. A* **2003**, *107*, 9147.

(39) (a) Knowles, P. J.; Hampel, C.; Werner, H. J. *J. Chem. Phys.* **1993**, *99*, 5219–5227 and references therein. (b) Knowles, P. J.; Hampel, C.; Werner, H. J. *J. Chem. Phys.* **2000**, *112*, 3106–7. (c) Watts, J. D.; Gauss, J.; Bartlett, R. J. *J. Chem. Phys.* **1993**, *98*, 8718.

(40) Chen, W.; Schlegel, H. B. *J. Chem. Phys.* **1994**, *101*, 5957–5968.

(41) Knowles, P. J.; Andrews, J. S.; Amos, R. D.; Handy, N. C.; Pople, J. A. *Chem. Phys. Lett.* **1991**, *186*, 130.

(42) Mokrushin, V.; Bedanov, V.; Tsang, W.; Zachariah, M.; Knyazev, V. *ChemRate*, version 1.19; NIST: Gaithersburg, MD, 2002.

(43) Miller, W. H. *J. Am. Chem. Soc.* **1979**, *101*, 6810.

(44) Eckart, C. *Phys. Rev.* **1930**, *35*, 1303.

(45) Knyazev, V. D. *J. Phys. Chem. A* **1998**, *102*, 3916.

(46) Pitzer, K. S.; Gwinn, W. D. *J. Chem. Phys.* **1942**, *10*, 428–440.

(47) Reid, R. C.; Prausnitz, J. M.; Sherwood, T. K. *The Properties of Gases and Liquids*, 3rd ed.; McGraw-Hill: New York, 1977.

(48) Wang, H.; Frenklach, M. *Combust. Flame* **1994**, *96*, 163.

(49) Wilkinson, J. H.; Reinsch, C. *Linear Algebra*; Springer: New York, 1971.

(50) (a) Bedanov, V. M.; Tsang, W.; Zachariah, M. R. *J. Phys. Chem.* **1995**, *99*, 11452. (b) Tsang, W.; Bedanov, V.; Zachariah, M. R. *J. Phys. Chem.* **1996**, *100*, 4011. (c) Knyazev, V. D.; Tsang, W. *J. Phys. Chem. A*

2000, *104*, 10747-10765. (d) Knyazev, V. D.; Tsang, W. *J. Phys. Chem. A* **1999**, *103*, 3944–3954.

(51) (a) Urry, W. H.; Kharash, M. S. *J. Am. Chem. Soc.* **1944**, *66*, 1438–1440. (b) Slaugh, L. H. *J. Am. Chem. Soc.* **1959**, *81*, 2262–2266. (c) Effio, A.; Griller, D.; Ingold, K. U.; Scaiano, J. C.; Sheng, S. J. *J. Am. Chem. Soc.* **1980**, *102*, 6063–6068.

(52) Asensio, A.; Dannenberg, J. J. *J. Org. Chem.* **2001**, *66*, 5996–5999.

(53) Korth, H. G.; Sustmann, R.; Sicking, W.; Klaerner, F. G.; Tashtoush, H. I. *Chem. Ber.* **1993**, *126*, 1917–1927.

(54) Van Speybroeck, V.; Van Neck, D.; Waroquier, M.; Wauters, S.; Saeys, M.; Marin, G. B. *J. Phys. Chem. A* **2000**, *104*, 10939–10950.

(55) (a) Van Speybroeck, V.; Borremans, Y.; Van Neck, D.; Waroquier, M.; Wauters, S.; Saeys, M.; Marin, G. B. *J. Phys. Chem. A* **2001**, *105*, 7713–7723. (b) Van Speybroeck, V.; Van Neck, D.; Waroquier, M. *J. Phys. Chem. A* **2002**, *106*, 8945–8950. (c) Van Speybroeck, V.; Van Neck, D.; Waroquier, M.; Wauters, S.; Saeys, M.; Marin, G. B. *Int. J. Chem. Kinet.* **2003**, *91*, 384–388.

(56) Conradi, M. S.; Zeldes, H.; Livingston, R. *J. Phys. Chem.* **1979**, *83*, 2160.

(57) Sancho-Garcia, J. C.; Perez-Jimenez, A. J. *J. Phys. B: At. Mol. Opt. Phys.* **2002**, *35*, 1509–1523 and references therein.

(58) Frenkel, M.; Marsh, K. N.; Wilhoit, R. C.; Kabo, G. J.; Roganov, G. N. *Thermodynamics of Organic Compounds in the Gas State*; Thermodynamics Research Center: College Station, TX, 1994.

(59) *NIST Chemistry WebBook*; NIST Standard Reference Database Number 69; Linstrom, P. J., Mallard, W. G., Eds.; National Institute of Standards and Technology: Gaithersburg, MD, March 2003 (http://webbook.nist.gov).

(60) Berkowitz, J.; Ellison, G. B.; Gutman, D. *J. Phys. Chem.* **1994**, *98*, 2744.

(61) Seakins, P. W.; Pilling, M. J.; Niiranen, J. T.; Gutman, D.; Krasnoperov, L. N. *J. Phys. Chem.* **1992**, *96*, 9847.

(62) Seetula, J. A. *Phys. Chem. Chem. Phys.* **2000**, *2*, 3807–3812.

(63) Marshall, P. *J. Phys. Chem. A* **1999**, *103*, 4560–4563.

(64) Ervin, K. M.; DeTuri, V. F. *J. Phys. Chem. A* **2002**, *106*, 9947–9956.

(65) Ervin, K. M.; Gronert, S.; Barlow, S. E.; Gilles, M. K.; Harrison, A. G.; Bierbaum, V. M.; DePuy, C. H.; Lineberger, W. C; Ellison, G. B. *J. Am. Chem. Soc.* **1990**, *112*, 5750.

(66) Davico, G. E.; Bierbaum, V. M.; DePuy, C. H.; Ellison, G. B.; Squires, R. R. *J. Am. Chem. Soc.* **1995**, *117*, 2590–9.

(67) Ellison, G. B.; Davico, G. E.; Bierbaum, V. M.; DePuy, C. H. *Int. J. Mass Spectrom. Ion Proc*esses **1996**, *156*, 109–131 and references therein.

(68) Song, S.; Golden, D. M.; Hanson, R. K.; Bowman, C. T. *J. Phys. Chem. A* **2002**, *106*, 6094–6098.

(69) Hippler, H.; Troe, J. *J. Phys. Chem.* **1990**, *94*, 3803.

(70) Walker, J. A.; Tsang, W. *J. Phys. Chem.* **1990**, *94*, 3324.

(71) Muralha, V. S. F.; Borges dos Santos, R. M.; Martinho Simoes, J. A. *J. Phys. Chem. A* **2004**, *108*, 936–942.

(72) Henry, D. J.; Parkinson, C. J.; Radom, L. *J. Phys. Chem. A* **2002**, *106*, 7927–7936.

(73) Orlov, Yu. D.; Bouchoux, G.; Takhistov, V. V.; Ponomarev, D. A. *J. Mol. Struct.* **2002**, *608*, 109–122.

(74) Orlov, Yu. D.; Lavrov, V. O.; Lebedev, Yu. A. *Russ. Chem. Bull.* **2001**, *50*, 963–969.

(75) Pokidova, T. S.; Denisov, E. T. *Kinet. Catal.* **2001**, *42*, 729–735.

(76) Zhang, X. M. *J. Org. Chem.* **1998**, *63*, 1872–1877.

(77) Yu, T.; Lin, M. C.; Melius, C. F. *Int. J. Chem. Kinet.* **1994**, *26*, 1095–104.

(78) Nicovich, J. M.; Ravishankara, A. R. *J. Phys. Chem.* **1984**, *88*, 2534.

(79) Hoyermann, K.; Preuss, A. W.; Wagner, H. Gg. *Ber. Bunsen-Ges. Phys. Chem.* **1975**, *79*, 156.

(80) Yang, K. *J. Am. Chem. Soc.* **1962**, *84*, 3795.

(81) Kim, P.; Lee, J. H.; Bonanno, R. J.; Timmons, R. B. *J. Chem. Phys.* **1973**, *59*, 4593.

(82) (a) Sauer, M. C., Jr.; Mani, I. *J. Phys. Chem.* **1970**, *74*, 59. (b) Sauer, M. C., Jr.; Ward, B. *J. Phys. Chem.* **1967**, *71*, 3971.

(83) To estimate the uncertainty in k_{R5}, we note that Park and Lin[16] reported the low-T experimental value of $k_{R5}(T = 300–500$ K) that is approximately twice the high-T value of Heckmann et al.[15] Given the weak dependence of the phenyl recombination rate constant on T, a factor of 2 uncertainty could be suggested for k_{R5}. We are not aware of any direct measurements of the k_{R4} rate constant at high T, but the assumed value of Stein et al.[12] agrees with the estimate of Colket et al.,[17] derived from modeling the acetylene pyrolysis at $T = 900–1100$ K. Benson's[18] and Tsang's[19] estimates are lower by a factor of 2, whereas the recent room-temperature experimental values of Fahr et al.[20] are higher by a factor of ~3. In the absence of the more reliable high-T kinetic data for reaction R4, we estimate a factor of 4 uncertainty in the original k_{R4} value used by Stein et al.[12]